and mediation (at least in part) of TGFβ1 activity. Periostin may also contribute to the pathogenesis of scleroderma via the proliferation and recruitment of myofibroblasts [17,24], enhancement of Notch1 signaling [29,45], and promotion of collagen assembly [10]. Thus, our observations and those of others collectively indicate that periostin is involved in the multiple steps of skin fibrosis and is an attractive target for the treatment of scleroderma.

We hope that our findings will contribute to both a better understanding of scleroderma pathogenesis and the development of novel therapeutic approaches, including the possible inhibition of periostin function, for the treatment of scleroderma.

## Materials and Methods

### Human Samples

The frozen biopsy tissues and paraffin-embedded tissue sections obtained from lesional skin of well-defined patients with diffuse systemic scleroderma (n = 12; male: female ratio 2:10, mean age 52.4 years [range 24–76 years]), lesional skin of patients with keloid (n = 8; male: female ratio 2:4, mean age 48.5 years [range 21–68 years]), hypertrophic scar (n = 7; male: female ratio 2:5, mean age 50.5 years [range 34–72 years]), and corresponding sites of healthy donors (n = 12; male: female ratio 3:9, mean age 49.2 years [range 26–65 years]) were used in this study. Written informed consent was obtained from all participants prior to study inclusion. The study was approved by the Medical Ethics Committee of Osaka University (Case number 2011-3/17-10193).

### Rearing Management of Animals

WT mice (C57BL/6 strain) were obtained from CLEA Japan, Inc. (Osaka, Japan). Periostin gene knockout ($PN^{-/-}$) mice (C57BL/6 strain) were generated as previously described [27]. All animal care and experimentation were performed in accordance with the institutional guidelines of the National Institute of Biomedical Innovation, Osaka, Japan (NIBIO) (Approval No. DS2147R1).

### BLM-induced Scleroderma Model and Tissue Sample Preparation

BLM (Nippon Kayaku, Tokyo, Japan) was dissolved in phosphate-buffered saline (PBS) at a concentration of 1 mg/ml and sterilized by filtration. BLM or PBS (100 μl) was injected subcutaneously as described by us previously [46]; one day after the final injection, the skin at the injected site was removed and processed for analysis as previously described [47].

### Histopathological Analysis, Assessment of Skin Thickness, and Collagen Synthesis

Paraffin-embedded tissue sections were stained with hematoxylin and eosin (H&E Fisher Scientific), and dermal thickness was calculated as described previously [48]. To assess dermal collagen deposition, semi-quantitative analysis using Masson's trichrome staining, in which collagen fibers are stained blue, was used. Collagen deposition was graded by examining five randomly chosen fields at 100× magnification in a blinded manner using three observers. The grading criteria were as follows: grade 0 = no collagen fibers; grade 1 = few collagen fibers; grade 2 = moderate amount of collagen fibers; and grade 3 = excessive amount of collagen fibers.

### Immunohistochemistry and Immunofluorescence Staining

Paraffin sections were prepared as referred to above and then subjected to immunohistochemistry and immunofluorescence staining as described previously [47,49]. The primary antibodies used were rabbit anti-periostin (1:3,000 dilution; Abcam, Cambridge, MA), mouse anti α-smooth muscle actin (α-SMA; 1:3,000 dilution; Sigma-Aldrich, St. Louis, MO) and rat anti-CD34 antibody (1:50 dilution; Abcam, Cambridge, MA), followed by the DAKO LSAP+System-AP (DakoCytomation) and Dako ChemMate Envision kit/HRP(DAB), or followed by the secondary antibody (anti-mouse Alexa Fluor 555, anti-rat Alexa Fluor 488, Invitrogen). The slides were visualized using a light microscope or Keyence Biozero confocal microscope. α-SMA-positive spindle cells (α-$SMA^+$ cells) or α-SMA-positive and CD34-negative spindle-shaped cells (α-$SMA^+$ $CD34^-$ cells) were counted in 10 non-contiguous random grids under high-power magnification fields (400×) by confocal microscope. Results are expressed as the mean ± standard deviation (SD) of positive spindle-shaped fibroblasts per field.

### Cell Culture

Neonatal murine primary dermal fibroblasts were isolated from the skin of 10-day-old WT mice and cultured as previously described [47]. After 24 hours of serum starvation, dermal fibroblasts were treated with TGFβ1 (2–12 ng/ml) or recombinant mouse periostin (rmPeriostin) (5–1,000 ng/ml) for the indicated periods prior to extraction of RNA and protein extraction. Cells were used at passage three. In each experiment, obtained fibroblasts were examined at the same time and under the same culture conditions (e.g., cell density, passage, and days after plating).

### Neutralizing and Kinase Inhibition Assays

Cells were grown on 6-well plates; after extensive washing with PBS to remove all sera, cells were serum-starved for 24 hours. Subsequently, the cells were incubated for 2 hours with the neutralizing antibody against αv-integrin (anti-αv-integrin Ab, Biolegend, San Diego, CA) and kinase inhibitors (Cell Signaling Technology, Beverly, MA) at the indicated concentrations: anti-αv-integrin Ab (10 μg/ml), genistein (10 μM), LY294002 (10 μM), PD98095 (50 μM), U0126 (20 μM), SB203580 (25 μM), temsirolimus (10 μM), and rapamycin (500 nM). Cells were then stimulated for 2 hours with 100 ng/ml rmPeriostin in the same media. After stimulation, total RNA was isolated. To analyze protein phosphorylation, cells were collected after five minutes of periostin stimulation. We performed a serial dilution to identify the optimal concentration of each inhibitor prior to the initiation of experiments by MTT assay and western blotting analysis, the nontoxic and effective concentration was used in neutralizing and kinase inhibition assay.

### RNA Isolation and Real-time Quantitative Polymerase Chain Reaction (PCR)

Total RNA from mouse skin tissues or cultured fibroblast cell pellets was isolated with RNeasy spin columns (Qiagen, Valencia, CA) following the manufacturer's instructions. The integrity of the RNA was verified by gel electrophoresis. Total RNA (100 ng) was reverse-transcribed into first-strand complementary DNA (cDNA) (QuantiTect Reverse Transcription Kit, Qiagen). The primers used for real-time PCR were as follows: TGFβ1, sense 5′-cgaatgtctgacgtattgaagaaca-3′, antisense 5′-ggagcccgaagcggacta-3′; CCN2/CTGF, sense 5′-caaagcagctgcaaatacca-3′, antisense 5′-gacaggcttggcgattttag-3′; α-SMA, sense 5′-tctctatgctaa-caacgtcctgtca-3′, antisense 5′-ccaccgatccagacagagtactt-3′; collagen type-I alpha 1 (Col1α1), sense 5′-gagccctcgcttccgtactc-3′, antisense 5′-tgttccctactcagccgtctgt-3′; and GAPDH, sense 5′-tgtcatca-

tacttggcaggtttct-3′, antisense 5′-catggccttccgtgttccta-3′. Each reaction was performed in triplicate. Variation within samples was less than 10%. Statistical analysis was performed with the Student's paired *t* test.

### Western Blotting Analysis

Proteins from skin samples and cell pellets were extracted, and 5 μg of extracted protein was used for western blotting analysis as described previously [47]. The primary antibodies were used at the following dilutions: anti-α-SMA (Sigma-Aldrich), 1:500; anti-periostin (R&D Systems. Minneapolis, MN), 1:500; anti-periostin (Abcam, Cambridge, MA), 1:1,000; anti-phospho-Akt (Cell Signaling Technology, Beverly, MA), 1:1,000; anti-Total Akt (Cell Signaling Technology), 1:1,000; and anti-GAPDH (Santa Cruz Biotechnology, Santa Cruz, CA), 1:500. We used anti-GAPDH antibody as a loading control.

### Statistical Analysis

The data were expressed as the mean ± SD. The Student's two-tailed *t*-test (Microsoft Excel software, Redmond, WA) was used for comparison between two groups. When analysis included more than two groups, one-way analysis of variance was used. P-values less than 0.05 were considered statistically significant.

## Supporting Information

**Figure S1 TGFβ1 does not affect cell viability of WT and $PN^{-/-}$ dermal fibroblasts.** Cell viabilities of WT and $PN^{-/-}$ dermal fibroblasts were assessed by MTT assay after treatment with TGFβ1 (5 ng/ml) for 2–24 hours. Data are shown as mean ± SD. NS, no significance.
(TIF)

**Figure S2 Periostin is induced by TGFβ1 in WT dermal fibroblasts in a dose- and time-dependent manner.** A, Real-time quantitative PCR was performed to determine relative mRNA levels of periostin in cultured WT dermal fibroblasts at two hours after TGFβ1 treatment at the indicated concentrations. B, Western blotting analysis for periostin with protein extracted from WT dermal fibroblasts or culture supernatants after TGFβ1 treatment at the indicated times. Values in A were normalized to GAPDH levels and expressed as relative mRNA levels compared with WT dermal fibroblasts without TGFβ1 treatment. Values in A are shown as the mean ± SD. NS, no significance; ***, $p<0.01$.
(TIF)

**Figure S3 The effects of TGFβ1 in the induction of α-SMA and Col1α1 were recovered by addition of rmPeriostin to cultured $PN^{-/-}$ fibroblasts.** Real-time quantitative PCR was performed to determine relative mRNA levels of α-SMA (A) and Col1α1 (B) in cultured dermal fibroblasts at 24 hours after TGFβ1 treatment. Values in A and B were normalized to GAPDH levels and expressed as relative mRNA levels compared with WT dermal fibroblasts without TGFβ1 treatment. Values in A and B are shown as the mean ± SD. NS, no significance; ***, $p<0.01$. (Note: Data of WT and $PN^{-/-}$ group shown here and those presented in Figure 5A and 6A are from the same data set.)
(TIF)

**Text S1 Supplementary materials and methods.**
(DOC)

## Acknowledgments

We acknowledge Laboratory of Animal Models for Human Diseases (National Institute of Biomedical Innovation, Osaka, Japan) for animal care and husbandry, Dr. Kenju Nishida for tissue processing and embedding, Dr. Barry Ripley for evaluation of the manuscript.

## Author Contributions

Conceived and designed the experiments: LY SS HM MF AK TN IK. Performed the experiments: LY SS HM MF MT SM YK SK. Analyzed the data: LY SS HM MF MT YK SK. Contributed reagents/materials/analysis tools: AK MT SM YK SK. Wrote the paper: LY SS HM MF.

## References

1. Gabrielli A, Avvedimento EV, Krieg T (2009) Scleroderma. N Engl J Med 360: 1989–2003.
2. Leask A, Abraham DJ, Finlay DR, Holmes A, Pennington D, et al. (2002) Dysregulation of transforming growth factor beta signaling in scleroderma: overexpression of endoglin in cutaneous scleroderma fibroblasts. Arthritis Rheum 46: 1857–1865.
3. Leask A (2009) Signaling in fibrosis: targeting the TGF beta, endothelin-1 and CCN2 axis in scleroderma. Front Biosci (Elite Ed) 1: 115–122.
4. Liu S, Shi-wen X, Abraham DJ, Leask A (2011) CCN2 is required for bleomycin-induced skin fibrosis in mice. Arthritis Rheum 63: 239–246.
5. Jun JI, Lau LF (2010) The matricellular protein CCN1 induces fibroblast senescence and restricts fibrosis in cutaneous wound healing. Nat Cell Biol 12: 676–685.
6. Liu S, Kapoor M, Denton CP, Abraham DJ, Leask A (2009) Loss of beta1 integrin in mouse fibroblasts results in resistance to skin scleroderma in a mouse model. Arthritis Rheum 60: 2817–2821.
7. Takeshita S, Kikuno R, Tezuka K, Amann E (1993) Osteoblast-specific factor 2: cloning of a putative bone adhesion protein with homology with the insect protein fasciclin I. Biochem J 294 (Pt 1): 271–278.
8. Kudo A (2011) Periostin in fibrillogenesis for tissue regeneration: periostin actions inside and outside the cell. Cell Mol Life Sci 68: 3201–3207.
9. Kii I, Amizuka N, Minqi L, Kitajima S, Saga Y, et al. (2006) Periostin is an extracellular matrix protein required for eruption of incisors in mice. Biochem Biophys Res Commun 342: 766–772.
10. Norris RA, Damon B, Mironov V, Kasyanov V, Ramamurthi A, et al. (2007) Periostin regulates collagen fibrillogenesis and the biomechanical properties of connective tissues. J Cell Biochem 101: 695–711.
11. Chen CC, Lau LF (2009) Functions and mechanisms of action of CCN matricellular proteins. Int J Biochem Cell Biol 41: 771–783.
12. Gillan L, Matei D, Fishman DA, Gerbin CS, Karlan BY, et al. (2002) Periostin secreted by epithelial ovarian carcinoma is a ligand for alpha(V)beta(3) and alpha(V)beta(5) integrins and promotes cell motility. Cancer Res 62: 5358–5364.
13. Baril P, Gangeswaran R, Mahon PC, Caulee K, Kocher HM, et al. (2007) Periostin promotes invasiveness and resistance of pancreatic cancer cells to hypoxia-induced cell death: role of the beta4 integrin and the PI3k pathway. Oncogene 26: 2082–2094.
14. Ruan K, Bao S, Ouyang G (2009) The multifaceted role of periostin in tumorigenesis. Cell Mol Life Sci 66: 2219–2230.
15. Larsen M, Artym VV, Green JA, Yamada KM (2006) The matrix reorganized: extracellular matrix remodeling and integrin signaling. Curr Opin Cell Biol 18: 463–471.
16. Norris RA, Moreno-Rodriguez R, Hoffman S, Markwald RR (2009) The many facets of the matricelluar protein periostin during cardiac development, remodeling, and pathophysiology. J Cell Commun Signal 3: 275–286.
17. Shimazaki M, Nakamura K, Kii I, Kashima T, Amizuka N, et al. (2008) Periostin is essential for cardiac healing after acute myocardial infarction. J Exp Med 205: 295–303.
18. Tilman G, Mattiussi M, Brasseur F, van Baren N, Decottignies A (2007) Human periostin gene expression in normal tissues, tumors and melanoma: evidences for periostin production by both stromal and melanoma cells. Mol Cancer 6: 80.
19. Horiuchi K, Amizuka N, Takeshita S, Takamatsu H, Katsuura M, et al. (1999) Identification and characterization of a novel protein, periostin, with restricted expression to periosteum and periodontal ligament and increased expression by transforming growth factor beta. J Bone Miner Res 14: 1239–1249.
20. Takayama G, Arima K, Kanaji T, Toda S, Tanaka H, et al. (2006) Periostin: a novel component of subepithelial fibrosis of bronchial asthma downstream of IL-4 and IL-13 signals. J Allergy Clin Immunol 118: 98–104.
21. Kühn B, del Monte F, Hajjar RJ, Chang YS, Lebeche D, et al. (2007) Periostin induces proliferation of differentiated cardiomyocytes and promotes cardiac repair. Nat Med 13: 962–969.
22. Dorn GW (2007) Periostin and myocardial repair, regeneration, and recovery. N Engl J Med 357: 1552–1554.
23. Hamilton DW (2008) Functional role of periostin in development and wound repair: implications for connective tissue disease. J Cell Commun Signal 2: 9–17.

24. Ontsuka K, Kotobuki Y, Shiraishi H, Serada S, Ohta S, et al. (2012) Periostin, a matricellular protein, accelerates cutaneous wound repair by activating dermal fibroblasts. Exp Dermatol 21: 331–336.
25. Zhou HM, Wang J, Elliott C, Wen W, Hamilton DW, et al. (2010) Spatiotemporal expression of periostin during skin development and incisional wound healing: lessons for human fibrotic scar formation. J Cell Commun Signal 4: 99–107.
26. Oku E, Kanaji T, Takata Y, Oshima K, Seki R, et al. (2008) Periostin and bone marrow fibrosis. Int J Hematol 88: 57–63.
27. Shimazaki M, Kudo A (2008) Impaired capsule formation of tumors in periostin-null mice. Biochem Biophys Res Commun 367: 736–742.
28. Nishiyama T, Kii I, Kashima TG, Kikuchi Y, Ohazama A, et al. (2011) Delayed re-epithelialization in periostin-deficient mice during cutaneous wound healing. PLoS One 6: e18410.
29. Tkatchenko TV, Moreno-Rodriguez RA, Conway SJ, Molkentin JD, Markwald RR, et al. (2009) Lack of periostin leads to suppression of Notch1 signaling and calcific aortic valve disease. Physiol Genomics 39: 160–168.
30. Gordon ED, Sidhu SS, Wang ZE, Woodruff PG, Yuan S, et al. (2012) A protective role for periostin and TGF-β in IgE-mediated allergy and airway hyperresponsiveness. Clin Exp Allergy 42: 144–155.
31. Yamamoto T, Takagawa S, Katayama I, Yamazaki K, Hamazaki Y, et al. (1999) Animal model of sclerotic skin. I: Local injections of bleomycin induce sclerotic skin mimicking scleroderma. J Invest Dermatol 112: 456–462.
32. Yamamoto T, Kuroda M, Nishioka K (2000) Animal model of sclerotic skin. III: Histopathological comparison of bleomycin-induced scleroderma in various mice strains. Arch Dermatol Res 292: 535–541.
33. Desmoulière A, Geinoz A, Gabbiani F, Gabbiani G (1993) Transforming growth factor-beta 1 induces alpha-smooth muscle actin expression in granulation tissue myofibroblasts and in quiescent and growing cultured fibroblasts. J Cell Biol 122: 103–111.
34. Border WA, Noble NA (1994) Transforming growth factor beta in tissue fibrosis. N Engl J Med 331: 1286–1292.
35. Norris RA, Borg TK, Butcher JT, Baudino TA, Banerjee I, et al. (2008) Neonatal and adult cardiovascular pathophysiological remodeling and repair: developmental role of periostin. Ann N Y Acad Sci 1123: 30–40.
36. Oka T, Xu J, Kaiser RA, Melendez J, Hambleton M, et al. (2007) Genetic manipulation of periostin expression reveals a role in cardiac hypertrophy and ventricular remodeling. Circ Res 101: 313–321.
37. Elliott CG, Wang J, Guo X, Xu SW, Eastwood M, et al. (2012) Periostin modulates myofibroblast differentiation during full-thickness cutaneous wound repair. J Cell Sci 125: 121–132.
38. Shi-wen X, Stanton LA, Kennedy L, Pala D, Chen Y, et al. (2006) CCN2 is necessary for adhesive responses to transforming growth factor-beta1 in embryonic fibroblasts. J Biol Chem 281: 10715–10726.
39. Lygoe KA, Wall I, Stephens P, Lewis MP (2007) Role of vitronectin and fibronectin receptors in oral mucosal and dermal myofibroblast differentiation. Biol Cell 99: 601–614.
40. Snider P, Hinton RB, Moreno-Rodriguez RA, Wang J, Rogers R, et al. (2008) Periostin is required for maturation and extracellular matrix stabilization of noncardiomyocyte lineages of the heart. Circ Res 102: 752–760.
41. Sidhu SS, Yuan S, Innes AL, Kerr S, Woodruff PG, et al. (2010) Roles of epithelial cell-derived periostin in TGF-beta activation, collagen production, and collagen gel elasticity in asthma. Proc Natl Acad Sci U S A 107: 14170–14175.
42. Yamaguchi Y, Mann DM, Ruoslahti E (1990) Negative regulation of transforming growth factor-beta by the proteoglycan decorin. Nature 346: 281–284.
43. Ikonomidis JS, Hendrick JW, Parkhurst AM, Herron AR, Escobar PG, et al. (2005) Accelerated LV remodeling after myocardial infarction in TIMP-1-deficient mice: effects of exogenous MMP inhibition. Am J Physiol Heart Circ Physiol 288: H149–158.
44. McCann MR, Monemdjou R, Ghassemi-Kakroodi P, Fahmi H, Perez G, et al. (2011) mPGES-1 null mice are resistant to bleomycin-induced skin fibrosis. Arthritis Res Ther 13: R6.
45. Tanabe H, Takayama I, Nishiyama T, Shimazaki M, Kii I, et al. (2010) Periostin associates with Notch1 precursor to maintain Notch1 expression under a stress condition in mouse cells. PLoS One 5: e12234.
46. Kitaba S, Murota H, Terao M, Azukizawa H, Terabe F, et al. (2011) Blockade of Interleukin-6 Receptor Alleviates Disease in Mouse Model of Scleroderma. Am J Pathol.
47. Terao M, Murota H, Kitaba S, Katayama I (2010) Tumor necrosis factor-alpha processing inhibitor-1 inhibits skin fibrosis in a bleomycin-induced murine model of scleroderma. Exp Dermatol 19: 38–43.
48. Murota H, Hamasaki Y, Nakashima T, Yamamoto K, Katayama I, et al. (2003) Disruption of tumor necrosis factor receptor p55 impairs collagen turnover in experimentally induced sclerodermic skin fibroblasts. Arthritis Rheum 48: 1117–1125.
49. Terao M, Ishikawa A, Nakahara S, Kimura A, Kato A, et al. (2011) Enhanced epithelial-mesenchymal transition-like phenotype in N-acetylglucosaminyltransferase V transgenic mouse skin promotes wound healing. J Biol Chem 286: 28303–28311.

# Severe dermatitis with loss of epidermal Langerhans cells in human and mouse zinc deficiency

Tatsuyoshi Kawamura,[1] Youichi Ogawa,[1] Yuumi Nakamura,[1] Satoshi Nakamizo,[2] Yoshihiro Ohta,[3] Hajime Nakano,[4] Kenji Kabashima,[2] Ichiro Katayama,[5] Schuichi Koizumi,[6] Tatsuhiko Kodama,[3] Atsuhito Nakao,[7] and Shinji Shimada[1]

[1]Department of Dermatology, Faculty of Medicine, University of Yamanashi, Yamanashi, Japan. [2]Department of Dermatology, Kyoto University Graduate School of Medicine, Kyoto, Japan. [3]Laboratory for Systems Biology and Medicine, Research Center for Advanced Science and Technology, University of Tokyo, Tokyo, Japan. [4]Department of Dermatology, Hirosaki University Graduate School of Medicine, Hirosaki, Japan. [5]Department of Dermatology, Osaka University School of Medicine, Osaka, Japan. [6]Department of Pharmacology and [7]Department of Immunology, Faculty of Medicine, University of Yamanashi, Yamanashi, Japan.

**Zinc deficiency can be an inherited disorder, in which case it is known as acrodermatitis enteropathica (AE), or an acquired disorder caused by low dietary intake of zinc. Even though zinc deficiency diminishes cellular and humoral immunity, patients develop immunostimulating skin inflammation. Here, we have demonstrated that despite diminished allergic contact dermatitis in mice fed a zinc-deficient (ZD) diet, irritant contact dermatitis (ICD) in these mice was more severe and prolonged than that in controls. Further, histological examination of ICD lesions in ZD mice revealed subcorneal vacuolization and epidermal pallor, histological features of AE. Consistent with the fact that ATP release from chemically injured keratinocytes serves as a causative mediator of ICD, we found that the severe ICD response in ZD mice was attenuated by local injection of soluble nucleoside triphosphate diphosphohydrolase. In addition, skin tissue from ZD mice with ICD showed increased levels of ATP, as did cultured wild-type keratinocytes treated with chemical irritants and the zinc-chelating reagent TPEN. Interestingly, numbers of epidermal Langerhans cells (LCs), which play a protective role against ATP-mediated inflammatory signals, were decreased in ZD mice as well as samples from ZD patients. These findings suggest that upon exposure to irritants, aberrant ATP release from keratinocytes and impaired LC-dependent hydrolysis of nucleotides may be important in the pathogenesis of AE.**

## Introduction

Zinc (Zn) is a trace element essential for cell growth, development, and differentiation and is involved in maintaining the structure and function of over 300 different enzymes (1, 2). More than 2,000 transcription factors regulating gene expression require Zn for their structural integrity and binding to DNA (3). Recent studies revealed that Zn acts as an intracellular second messenger for transducing extracellular stimuli into intracellular signaling events in monocytes, DCs, and mast cells (4–7).

Zn deficiencies can be divided into 2 groups — a congenital form, called acrodermatitis enteropathica (AE; OMIM 201100), and the acquired forms (8). Recently, mutations in SLC39A4 have been identified as being responsible for congenital AE (9–11). SLC39A4 encodes ZIP4 Zn transporter, which is involved in Zn uptake via transporting Zn into the cytoplasm in intestine (9, 10). Congenital AE occurs worldwide, with an estimated incidence of 1 per 500,000 children, while it has been estimated that more than $2 \times 10^9$ people have a nutritional deficiency for Zn in developing countries (3, 8). It is even estimated that a considerable proportion of the Western population is at risk of marginal Zn deficiency (12, 13). Conditional Zn deficiencies also occur in many diseases and abnormal conditions, including malabsorption syndrome, chronic liver and renal diseases, sickle cell disease, excessive intake of alcohol, malignancies, and other chronic debilitating conditions (1, 3, 8).

The clinical manifestations of inherited and acquired Zn deficiency include growth retardation, diarrhea, alopecia, and characteristic skin lesions on acral, periorificial, and anogenital areas. Since Zn is indispensable for an adequate immunological response to all pathogens (14), the most serious complication observed in Zn deficiency is repeated infections due to impaired immune function. Indeed, several studies using animal models of Zn deficiency have confirmed that decreased levels of Zn induce thymic atrophy, lymphopenia, and compromised cell- and antibody-mediated immune responses (14, 15). Zn deficiency affects many aspects of immune function, including a shift of the Th cell response to a Th2 predominance, reduced antibody formation, reduced killing activity by NK cells and lower levels of phagocytosis and intracellular killing in granulocytes, monocytes, and macrophages (14–18). Zn also influences the production of chemokines and proinflammatory cytokines like TNF-α, IL-1β, and IL-6 (19–22).

The effects of Zn deficiency are particularly obvious in the skin and are seen as erythematous rashes, scaly plaques, and ulcers on acral and periorificial areas. Paradoxically, despite the impaired immune function in Zn deficiency, patients with hereditary and acquired AE present with immunostimulating skin inflammation, known as "acrodermatitis." It remains unclear which cellular processes induce this characteristic skin inflammation and account for the cutaneous pathological features of Zn deficiency (8). Here we investigated the mechanisms by which Zn deficiency induces dermatitis in AE using dietary Zn-deficient (ZD) mice.

**Conflict of interest:** The authors have declared that no conflict of interest exists.
**Citation for this article:** *J Clin Invest.* 2012;122(2):722–732. doi:10.1172/JCI58618.

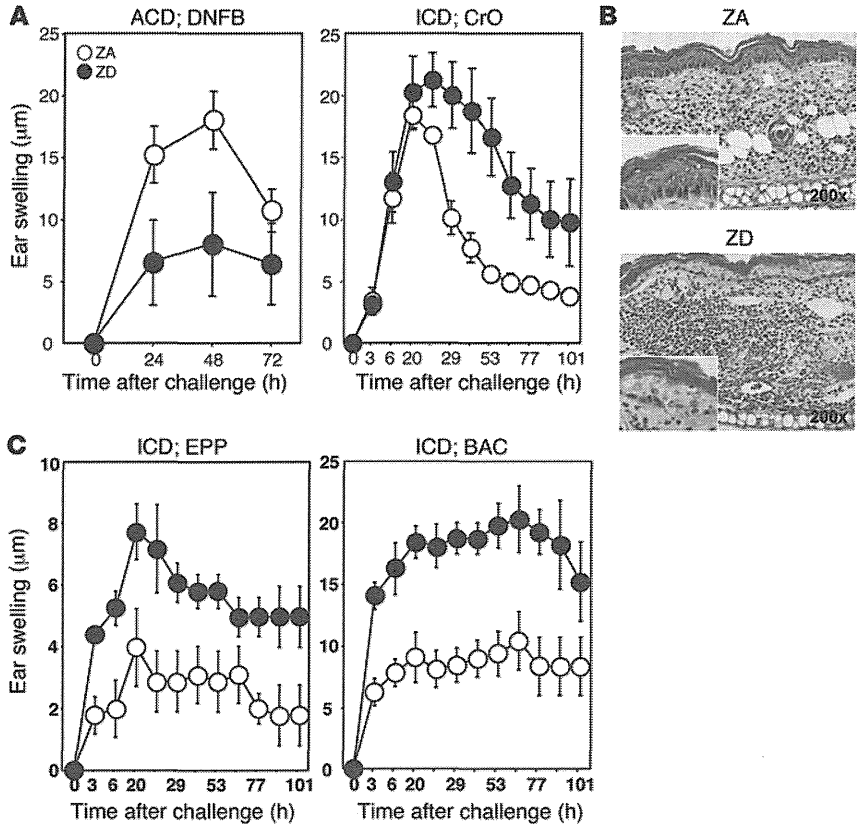


**Figure 1**
ZD mice demonstrate severe ICD with histological degeneration of keratinocytes. (**A** and **C**) ACD responses to DNFB and ICD responses to CrO, EPP, or BAC were induced in ZA (white circles) and ZD (black circles) mice, as described in Methods. Ear thickness was evaluated at the indicated time points. The data shown are ($n$ = 5) the swelling responses (mean ± SD). (**B**) H&E staining of ear samples collected from ZA or ZD mice 24 hours after topical application of CrO. Original magnification: ×200; ×400 (insets). Data are representative of 3 independent experiments.

## Results

*Dietary Zn deficiency causes severe and prolonged irritant contact dermatitis with the histological features of AE.* Symptoms of Zn deficiency in animals are similar across different species. Zn deficiency causes a well-characterized nutritional-immunological syndrome in mice (14–18, 23, 24), whereby young adults quickly manifest symptoms within 4 to 5 weeks of feeding a ZD diet containing 0.5 mg Zn/kg or more (23, 24). It is of note that, although ZD mice at approximately 70% to 80% of the control group weight exhibited visible cutaneous symptoms, such as alopecia and parakeratosis, they did not present with the characteristic inflammatory dermatitis of patients with AE (refs. 23, 24, and Supplemental Figure 1; supplemental material available online with this article; doi:10.1172/JCI58618DS1). Because AE in humans is typically seen on areas subject to repeated contact, we investigated allergic contact dermatitis (ACD) and irritant contact dermatitis (ICD) in dietary ZD mice. Five-week-old BALB/c mice were fed a ZD or Zn-adequate (ZA) diet, and at 10 weeks of age, ACD in response to dinitrofluorobenzene (DNFB) and ICD in response to croton oil (CrO) were quantified. Consistent with previous findings (24), ZD mice showed markedly decreased ear swelling responses to DNFB compared with those of ZA mice (Figure 1A). This was probably due to immunodeficiency in ZD mice, as previously reported (14, 15). Surprisingly, in contrast, the ear swelling response to CrO in ZD mice was significantly increased and prolonged compared with that of ZA mice (Figure 1A and Supplemental Figure 2). ICD caused by other skin irritant chemicals, benzalkonium chloride (BAC) and ethyl phenylpropiolate (EPP), was also tested, with similar results (Figure 1C and Supplemental Figure 2). Histological examination of ICD lesions in ZD mice revealed parakeratosis and cytoplasmic pallor, subcorneal vacuolization, and ballooning degeneration of keratinocytes and leukocyte infiltration (Figure 1B). These signs are histological features of cutaneous AE lesions in humans. No such degeneration of keratinocytes was observed in ICD lesions in ZA mice or ACD lesions in either ZA or ZD mice (Figure 1B and data not shown). These findings suggest that ICD, but not ACD, responses in ZD mice mimic the characteristic cutaneous manifestations observed in AE and can thus be considered an appropriate model for human disease.

*Zn deficiency increases ATP release from keratinocytes in response to irritants.* Accumulating evidence suggests that different environmental stimuli (e.g., chemical irritants) trigger adenosine 5′-triphosphate (ATP) release from keratinocytes via nonlytic mechanisms and also, more frequently, as a consequence of cell damage or acute cell death (25–27). Once released, ATP activates a family of plasma membrane receptors known as purinergic (P2) receptors. Because ATP released from chemically injured keratinocytes has been shown to cause ICD (28), we next compared the amount of ATP that was released from ZD or ZA mouse skin tissue after CrO application in ex vivo organ culture. Skin tissue obtained from ZD mice 4, 6, or 20 hours after CrO application released significantly greater amounts of ATP than tissues from ZA mice (Figure 2A). We next examined the effect of the Zn-chelating reagent TPEN on exogenous ATP release from Pam-212 keratinocytes cultured in vitro. Consistent with previous findings (26, 28), Pam-212 keratinocytes rapidly released ATP after exposure to CrO (Figure 2B). The addition of TPEN to the culture significantly augmented release of ATP in response to CrO, whereas TPEN alone failed to increase ATP release (Figure 2, B and D). The TPEN-mediated increase of ATP secretion was prevented by the addition of $ZnSO_4$ in a dose-dependent manner (Figure 2C). Furthermore, TPEN also significantly increased the secretion of ATP in response to other skin

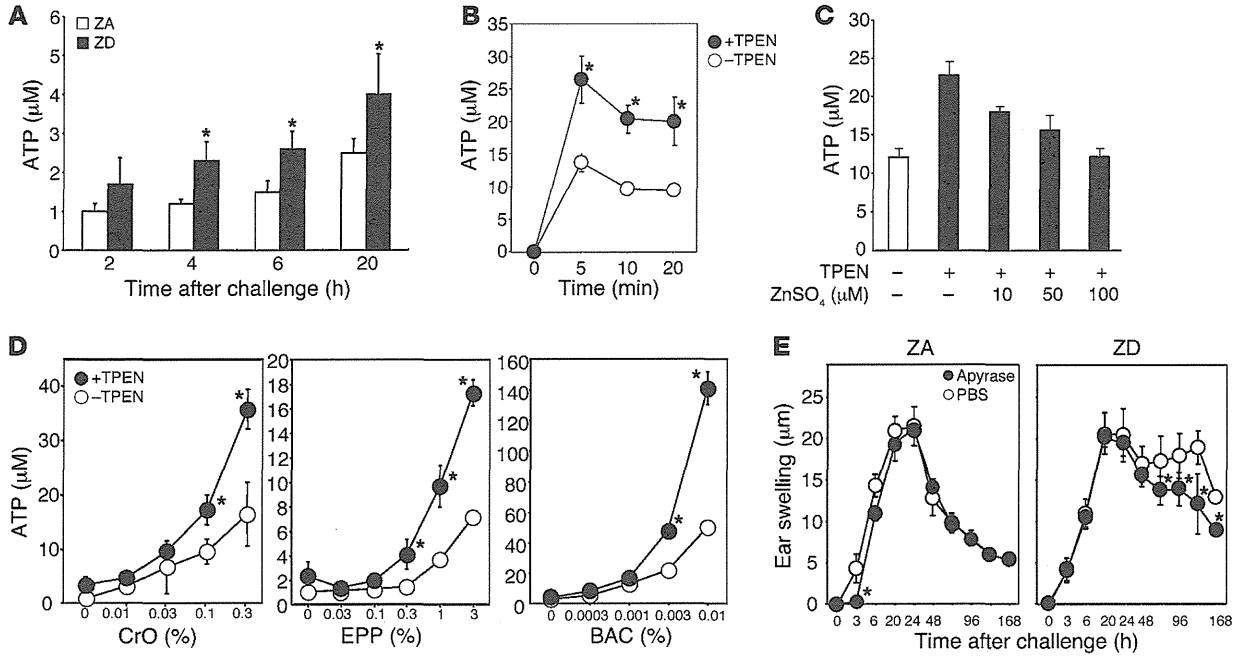


**Figure 2**

Zn deficiency increases ATP release by keratinocytes in response to irritant chemicals. (**A**) 1% CrO was painted on the ears of ZA (white bars) and ZD (black bars) mice ($n = 5$), and skin samples were taken at the indicated time points. ATP secretion from skin organ cultures was quantified. (**B–D**) Pam-212 keratinocytes were treated with (**B** and **C**) 0.3% CrO or (**D**) titrated concentrations of CrO, EPP, or BAC in the presence (black circles/bars) or absence (white circles/bars) of 2 μM TPEN. ATP in the culture supernatants was quantified at (**B**) the indicated time points or (**C** and **D**) 10 minutes after stimulation. (**C**) Cells were cultured with 10–100 μM $ZnSO_4$. $^*P < 0.05$, compared with cells that were not treated with TPEN. (**E**) ICD responses to CrO were induced, as described in Figure 1. ZA and ZD mice ($n = 5$) received local injections of potato apyrase on the right ear (black circles) or PBS alone on the left ear (white circles) before and after CrO application to both ears. The data shown are the swelling responses (mean ± SD). $^*P < 0.05$, between the apyrase and PBS treatments. Data are representative of 3 independent experiments.

irritant chemicals (herein, EPP and BAC) (Figure 2D). Together, these findings clearly indicate that Zn deficiency and irritant chemicals synergistically increase ATP release from keratinocytes.

Although various types of cells release ATP, the mechanism underlying the release of ATP is controversial (29). Several studies have shown that the release of ATP is reduced by carbenoxolone (CBX), suggesting the involvement of connexin or pannexin membrane channels in the release. In addition, inhibition of ATP release by vesicular ATPase inhibitors or intracellular $Ca^{2+}$ deprivation was also reported, suggesting that the mechanisms of ATP release could include exocytosis. As shown in Supplemental Figure 3, CBX significantly decreased ATP release from CrO-treated keratinocytes, and, more importantly, it dramatically inhibited TPEN-mediated increase of ATP secretion. By contrast, BAPTA-AM, a membrane-permeable, strong $Ca^{2+}$-chelator, did not affect the CrO-evoked ATP release from keratinocytes. These results clearly indicate that membrane channel–mediated diffusible mechanisms, but not $Ca^{2+}$-dependent exocytosis, play a key role in the release of ATP from keratinocytes treated with CrO.

Previous studies have shown that hydrolysis of nucleotides by s.c. injections of soluble ecto-nucleoside triphosphate diphosphohydrolase (NTPDase; soluble potato apyrase) diminishes early inflammation in ICD (28). As shown in Figure 2E, we obtained similar results in ZA mice. In contrast, injections of apyrase before and after CrO application in ZD mice significantly decreased the late ICD response (Figure 2E). This suggests that aberrant ATP release from epidermal keratinocytes in response to irritant chemicals contributes, at least in part, to the prolonged ICD response in ZD mice.

*Aberrant chemokine gene expression in ZD keratinocytes.* In general, there are very few differences in the histological, immunohistochemical, and electron microscopy findings in ACD and ICD (30). However, ICD is thought to be mediated via T cell–independent innate immunity, because the ear swelling response to CrO is similar for both athymic and normal mice and neutrophils are the predominant cells in ICD (31). Recent work has shown that different patterns of inflammatory chemokines may distinguish between ACD and ICD (32). To explore such mechanisms for increased ICD in Zn deficiency, we first analyzed gene expression profiles for 44 chemokines in epidermal sheets obtained from ZA and ZD mice 24 hours after vehicle or CrO exposure. Profound differences in chemokine gene expression were observed (Supplemental Figure 4). However, *Cxcl1* was markedly induced by CrO in both ZA and ZD mice, suggesting a possible association between this chemokine and neutrophil recruitment. Because CXCL1 and CXCL2 are known to mediate neutrophil influx into tissues (33), we next quantified their mRNA expression in epidermal sheets obtained from ZA and ZD mice after vehicle or CrO application in vivo. Quantitative real-time PCR demonstrated that Zn deficiency resulted in a significant increase of *Cxcl1* mRNA 4 and 24 hours after CrO exposure and *Cxcl2* mRNA at 4 hours (Figure 3, A and B). The same enhancing effects of Zn deficiency for the chemokine mRNA expression were observed when mice were treated with BAC (Supplemental Figure 5A). In addition, in vitro exposure of Pam-

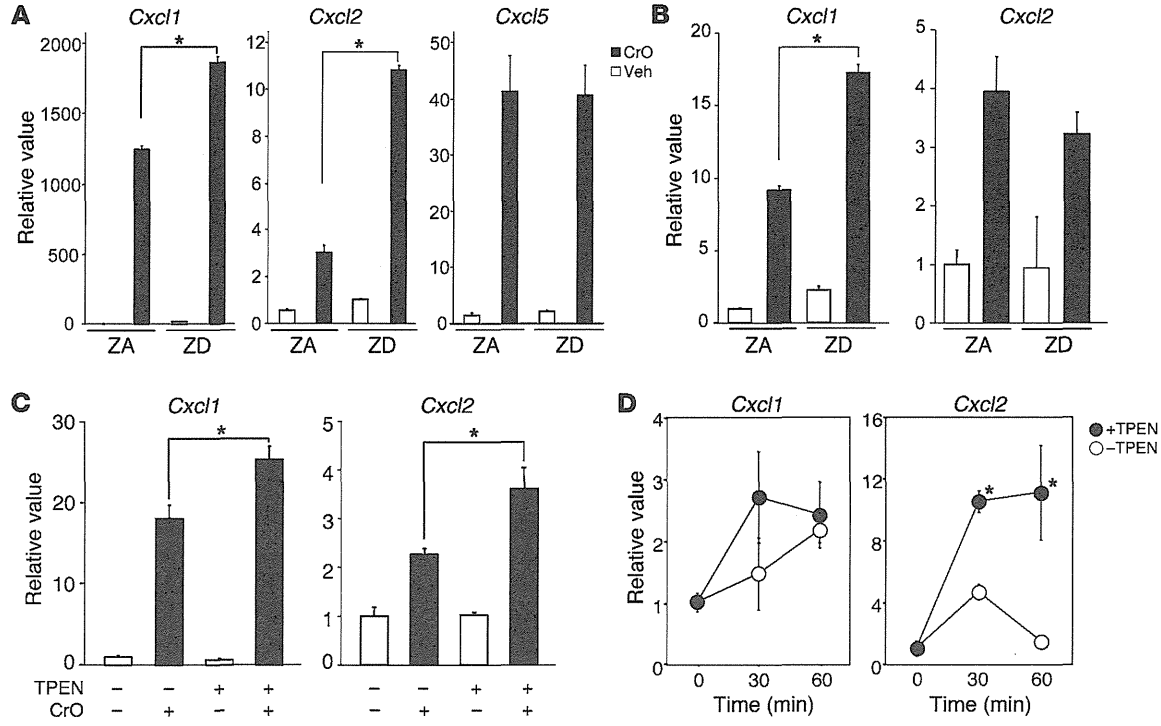


**Figure 3**

Zn deficiency increases *Cxcl1* and *Cxcl2* gene expression in keratinocytes after treatment with CrO. (**A** and **B**) 1% CrO (black bars) or vehicle alone (white bars) was painted on the ears of ZA and ZD mice ($n$ = 5). Epithelial sheets were obtained from the ears at (**A**) 4 hours or (**B**) 24 hours, and total RNA was extracted. (**C**) Pam-212 keratinocytes were cultured in the presence or absence of 2 μM TPEN. Total RNA was extracted 4 hours after 0.3% CrO (black bars) or vehicle (white bars) exposure. (**D**) Pam-212 keratinocytes were treated with 100 μM ATPγS in the presence (black circles) or absence (white circles) of 2 μM TPEN. Total RNA was extracted 4 hours after ATPγS exposure. Quantitative real-time RT-PCR analysis of *Cxcl1* and *Cxcl2* was performed. *Cxcl5* was examined as control in **A**. mRNA expression was normalized to *Gapdh*. The fold induction (mean ± SD) was calculated from the normalized mRNA expression by CrO- or ATP-stimulated keratinocytes relative to nonstimulated ZA keratinocytes. *$P$ < 0.05, compared with cells that were from ZA mice or not treated with TPEN. Data are representative of 3 independent experiments.

212 keratinocytes to CrO rapidly induced *Cxcl1* and *Cxcl2* mRNA (Figure 3C). When TPEN was added to the cultures, significant further augmentation of CrO-induced chemokine mRNA accumulation was observed, which was not seen with TPEN alone (Figure 3C). Similar results were obtained in BAC-treated keratinocytes (Supplemental Figure 5B). Furthermore, consistent with recent findings (34), exogenous ATPγS induced *Cxcl1* and *Cxcl2* mRNA expression by ZA Pam-212 keratinocytes (Figure 3D). Together, our results suggest that Zn deficiency indirectly augments *Cxcl1* and *Cxcl2* gene expression in CrO-stimulated keratinocytes via increased ATP release, as observed in Figure 2. Interestingly, Zn deficiency further augmented ATPγS-induced *Cxcl2*, but not *Cxcl1*, mRNA expression (Figure 3D).

*Loss of epidermal Langerhans cells in Zn deficiency.* Langerhans cells (LCs) are a long-lived subset of tissue DCs that reside in the epidermis. LCs acquire skin antigens and then migrate to skin-draining LNs in both inflammatory and steady-state conditions (35). Recently, it has been shown that CD39, which is expressed exclusively by LCs in the epidermal compartment, is responsible for ecto-NTPDase activity in LCs (28). Because the P2-receptor signaling pathway is negatively regulated by NTPDase-dependent hydrolysis of ATP, LC-associated CD39 plays a protective role against ATP-mediated inflammatory signals by hydrolyzing extracellular nucleotides released by keratinocytes in ICD responses (28). Therefore, we next examined the number, distribution, and morphology of epidermal LCs in Zn deficiency. Although epidermal cells prepared from the ear skin of ZA mice contained a normal contingent of LCs (I-$A^{d+}$ $CD11c^+$ cells), in mice fed the ZD diet, the number of epidermal LCs decreased with time on the diet, and few LCs were observed after 6 weeks (Figure 4, A and B). Immunofluorescence microscopy confirmed the loss of LCs from epidermal sheets prepared from mice fed a ZD diet for 6 weeks (Figure 4C). In contrast, the frequency and morphology of dendritic epidermal T cells (DETCs; $Thy\text{-}1^+$ cells), which are skin-resident γδ T cells expressing a monoclonal T cell receptor containing Vγ3 and Vδ1 determinants, in ZD mice was normal even after 6 weeks (Figure 4, C and D). It is of note that the proportions of I-$A^+$ $CD11c^+$ cells in axillary and inguinal lymph nodes, including migratory DCs (e.g., LCs) and resident lymphoid DCs, from ZD mice were comparable in number to those of ZA mice (Figure 4A). The possibility that Zn deficiency downregulates the expression of cell surface markers on epidermal LCs was considered unlikely, because treatment of epidermal sheets with TPEN (2 μM) for 4 days failed to decrease surface expression of I-$A^d$ and CD11c on murine epidermal LCs (data not shown).

*Loss of epidermal LCs in patients with AE.* We next examined the number, distribution, and morphology of epidermal LCs in human skin

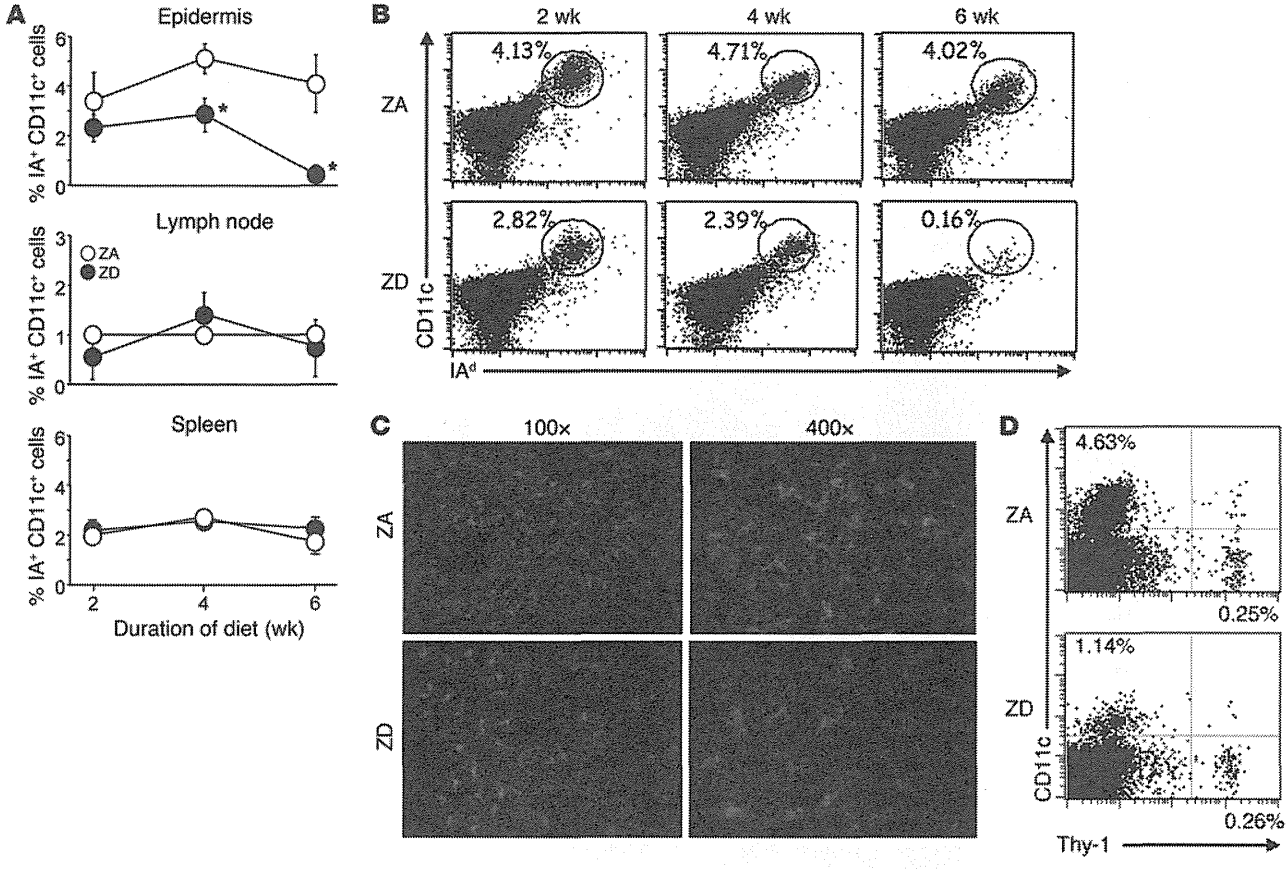


**Figure 4**

Loss of epidermal LCs in Zn deficiency. (**A**) Cell suspensions of epidermis, axillary, and inguinal lymph nodes and spleens were prepared from mice fed ZA (white circles) or ZD (black circles) diets for the indicated time and stained for I-A and CD11c antigens. The percentages of I-A and CD11c double-positive cells were assessed within each live-gated cell population. Results are the mean ± SD ($n$ = 3). *$P$ < 0.05, compared with mice fed the ZA diet. A representative FACS analysis of live-gated epidermal cell suspensions from mice fed ZA or ZD diets for 6 weeks and stained for (**B**) I-A and CD11c or (**D**) Thy-1 and CD11c antigens. Numbers indicate the percentages of cells in the (**B**) circles or (**D**) gate. (**C**) Immunofluorescence of epidermal whole mounts stained for I-A (red) and Thy-1 (green) from mice fed ZA or ZD diets for 6 weeks. Original magnification, ×100 (left panels); ×400 (right panels). Data are representative of 3 independent experiments.

samples obtained from inflammatory lesions of patients, including those with atopic dermatitis, psoriasis vulgaris, and hereditary and acquired AE, by immunofluorescence staining analyses. Langerin$^+$ LCs were found to be regularly scattered throughout the epidermis of control specimens but were absent from the epidermis of patients with AE (Figure 5A). HLA-DR antigens were also rarely expressed in the epidermis of AE specimens but were present on the surface of dermal mononuclear cells in the same specimens (Figure 5B). Interestingly, skin biopsy specimens obtained from the same lesions in a patient with hereditary AE after 6 months of oral Zn supplementation revealed recolonization of the epidermis with LCs, accompanied by marked clinical improvement (Figure 5C). We also examined immunohistochemical staining with formalin-fixed skin samples obtained from patients with AE. As shown in Supplemental Figure 6A, langerin$^+$ LCs were absent from the epidermis of the patients with AE. Quantitation of langerin$^+$ cells in the epidermis ($n$ = 3) revealed that the number of LCs in the lesional epidermis of AE specimens was significantly decreased as compared with that in normal skin (the mean positive cell per field ± SD was 16.7 ± 2.8 in normal skin and 0.4 ± 0.3 in AE skin; $P$ < 0.05). Similarly, the number of HLA-DR$^+$ cells in the lesional epidermis of AE specimens was also significantly decreased (the mean positive cell per field ± SD was 10.4 ± 0.6 in normal skin and 3.7 ± 2.7 in AE skin; $P$ < 0.05). Taken together with the findings in ZD mice (Figure 4), these findings indicate that Zn deficiency results in depletion of epidermal LCs.

*Decreased steady-state production of TGF-β1 in cutaneous, but not mucosal, epidermis in Zn deficiency.* Although the mechanisms that regulate LC homeostasis in the steady state are yet to be fully elucidated, previous studies demonstrated that LC development requires TGF-β1 (35). Mice lacking TGF-β1 possess no LCs, owing to either a failure in LC differentiation, survival, or both (35, 36). Therefore, we next assessed the cutaneous expression of TGF-β1 in Zn deficiency. Mucosal TGF-β1 levels in the large and small intestine in ZD mice were comparable to those in ZA mice (Figure 6B), whereas the skin tissue obtained from ZD mice contained significantly lower amounts of TGF-β1 than that from ZA mice (Figure 6A). To detect the TGF-β activity in the skin samples, MFB-F11 reporter cells were used in a bioassay (Figure 6C and ref. 37). Secreted alkaline phosphatase (SEAP) activity was not detected without activation of the samples by HCl, suggesting that murine skin contains TGF-β protein in a latent form. However, after activation, skin samples

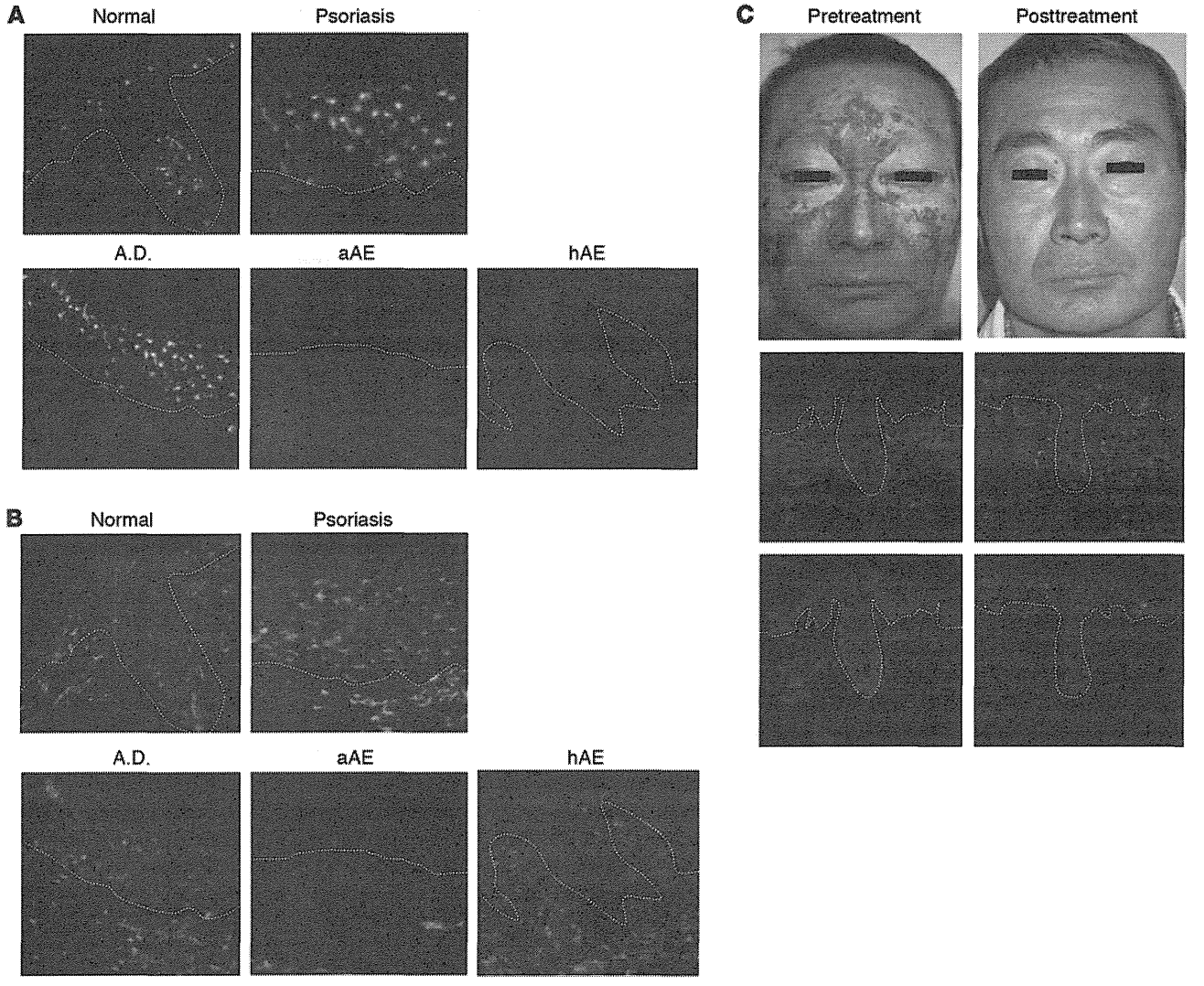


**Figure 5**
Loss of epidermal LCs in patients with AE. (**A** and **B**) Immunohistochemical staining for HLA-DR (green) and langerin (red) in the erythematous lesions of patients with psoriasis vulgaris (psoriasis), atopic dermatitis (A.D.), hereditary AE (hAE), and acquired AE (aAE) or normal skin. Original magnification, ×200. (**C**) Clinical appearance and immunohistochemical staining of a patient with hereditary AE before and after treatment by oral Zn supplement. White dotted lines denote the epidermis/dermis interface. Original magnification, ×200.

obtained from ZD mice were found to mediate significantly less SEAP activity than those from ZA mice (Figure 6C). In addition, we found that *Tgfb1* mRNA levels in epidermal sheets from ZD mice were significantly lower than those from ZA mice (Figure 6D). These results suggest that Zn deficiency decreases epidermal TGF-β1 expression in the steady state, and this might, at least in part, be associated with the reduction of epidermal LCs in Zn deficiency.

Because recent studies have shown that TGF-β1 has antiapoptosis effects in LCs or DCs (38, 39), we next assessed for apoptosis in epidermal LCs freshly isolated from ZA and ZD mice. As shown in Supplemental Figure 7A, the incidence of annexin $V^+$ cells in LCs from mice fed ZD diets for 3 weeks was slightly, but significantly, higher than that from mice fed ZA diets. We next performed in vitro experiments to obtain additional evidence for the hypothesis that Zn deficiency directly induces apoptosis of LCs. After in vitro culture of epidermal cell suspensions obtained from ZA mice with varying concentrations of TPEN for 48 hours, 5 μM TPEN significantly increased the incidence of annexin $V^+$ LCs (Supplemental Figure 7B). Similarly, we also found a significant increase of apoptosis in human monocyte-derived LCs cultured with TPEN at a concentration of 5 μM (Supplemental Figure 7C). Notably, consistent with a previous finding in HaCaT keratinocytes (40), Pam-212 keratinocytes cultured with 5 μM TPEN for 48 hours demonstrated no changes in cell viability and growth (data not shown). These results suggest that, in addition to the reduced TGF-β1 in epidermis, severe Zn deficiency may directly induce apoptosis in LCs, resulting in the loss of LC networks in ZD mice.

*Enhanced ICD in the absence of LCs.* At present, there are 2 types of LC ablation murine models. The first LC ablation model uses transgenic langerin$^-$ diphtheria toxin A (DTA) mice (41), which constitutively lack LCs. The second uses mice that express EGFP fused with a diphtheria toxin receptor (DTR) under the control

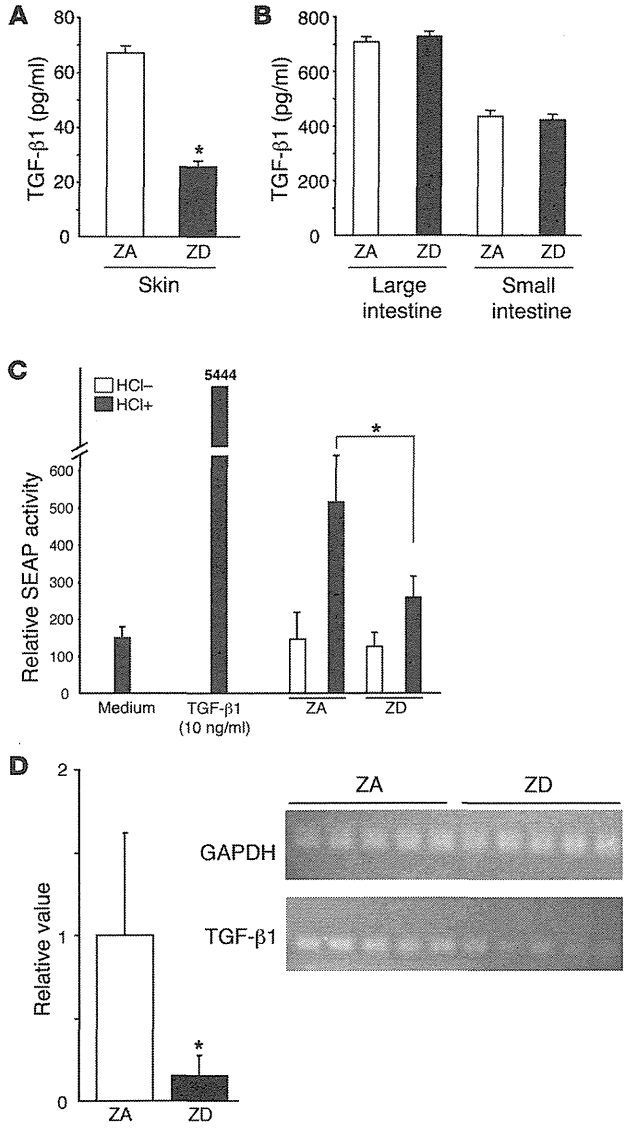


**Figure 6**

Decreased TGF-β1 production in the skin of ZD mice. (**A** and **B**) Samples of (**A**) skin tissue or (**B**) mucosal tissue were taken from the backs of mice fed a ZA (white bars) or ZD (black bars) diet for 5 weeks and cultured for 24 hours ($n = 5$). TGF-β1 secretion in the ex vivo skin or mucosa organ cultures was assessed by ELISA assays. (**C**) SEAP activity of the skin samples measured using MFB-F11 cells with or without HCl in the culture system. (**D**) Quantitative real-time RT-PCR for the detection of *Tgfb1* and *Gapdh* mRNAs in epidermis from the ears of mice fed a ZA (white bar) or ZD (black bar) diet for 5 weeks. The fold induction was calculated from normalized mRNA expression by the epidermis of ZD mice relative to that of ZA mice. Results are the mean ± SD ($n = 5$). *$P < 0.05$, compared with mice fed the ZA diet. Data are representative of several experiments with similar results.

of the langerin promoter, which are known as langerin-EGFP-DTR mice (42) and langerin-DTR mice (43). After i.p. injection of diphtheria toxin (DT) into langerin-EGFP-DTR mice, LCs do not repopulate for at least 4 weeks, while the number of langerin$^+$ dermal DCs in the skin recover to the basal level about 7 days after depletion by DT (44). Langerin-EGFP-DTR mice 14 days after treatment with DT are used as a model to deplete LCs alone. Fourteen days after treatment with DT, langerin-DTR mice and C57BL/6 (B6) mice were treated with 5%, 1%, and 0.5% CrO on the ears and monitored for ear swelling. As expected, the ear swelling response to 1% and 0.5% CrO in langerin-DTR mice was significantly increased at 12 and 24 hours after application compared with that in corresponding B6 mice (Figure 7). These results suggest that depletion of LCs enhances ICD responses, consistent with our findings that ZD mice lacking epidermal LCs exhibited increased ICD responses to 1% CrO (Figures 1 and 4).

## Discussion

Although the skin is commonly involved and is often one of the first organs affected in Zn deficiency, the underlying pathophysiology of the inflammatory skin manifestation in AE remains unclear. Nearly pathognomonic in the histopathologic examination of AE is the presence of "necrolysis," a term describing cytoplasmic pallor, vacuolization, ballooning degeneration, and subsequent confluent necrosis of keratinocytes within the epidermis (8). As several in vitro studies have shown that Zn deficiency can induce cell death in HaCaT keratinocytes via apoptosis or necrosis (40, 45, 46), one of the mechanisms of epithelial damage observed in AE lesions might be by increased death of keratinocytes. However, the characteristic inflammatory dermatitis in clinical AE is seen only in the acral areas, suggesting the participation of additional cellular processes, which could account for the restricted localization of the dermatitis and the severe cutaneous inflammation in immunodeficient AE patients.

Our data, which we believe to be novel, reveal that irritants, but not haptens, can cause severe skin inflammation in immunodeficient ZD mice, providing a biologic basis for understanding the pathogenesis of AE. We found that ICD responses in ZD mice exhibited similar histological features similar to those of the characteristic dermatitis in clinical AE, highlighting the possibility that the acral, periorificial, and anogenital dermatitis in AE might be caused by contact with different irritants in daily life, such as chemicals, foods, urine, and feces, etc. We have addressed the mechanisms responsible for the severe and prolonged ICD in ZD mice and have identified several abnormalities which we believe to be novel, including aberrant chemokine gene expression and ATP release by keratinocytes in response to irritant chemicals. These 2 abnormalities are closely associated, because extracellular ATP induces keratinocyte *Cxcl1* and *Cxcl2* gene expression, major chemoattractants for neutrophils (Figure 3D and refs. 33, 34). Together with the insight that neutrophils are the pathogenic cells in ICD (31), our results suggest that ATP plays a key role in the pathogenesis of severe and prolonged ICD in Zn deficiency. This notion is supported by the finding that local injection of apyrase significantly diminished the ICD response in ZD mice (Figure 2E). Our in vitro assay revealed that membrane channel–mediated diffusible mechanisms play a pivotal role in the Zn deficiency–induced increased ATP release from irritant-stimulated keratinocytes (Supplemental Figure 3). However, because chemical irritants also trigger ATP release from keratinocytes as a consequence of cell damage or acute cell death (26, 28), Zn deficiency and irritants may synergistically induce keratinocyte cell damage, as shown in Figure 1B, leading to increased ATP release in vivo.

We found that ex vivo ATP release from CrO-treated skin was increased in Zn deficiency (Figure 2A). This observation is in line

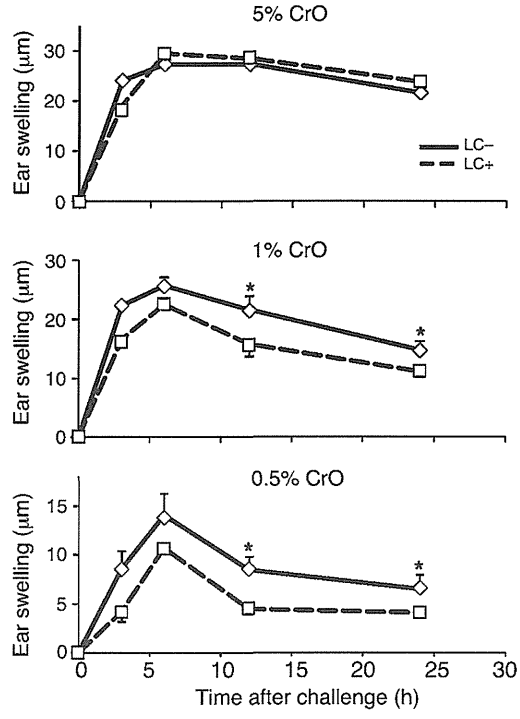


**Figure 7**
Enhanced ICD in the absence of LCs. Fourteen days after treatment with DT, langerin-DTR (LC–) and B6 (LC+) mice were applied with 5% (mean ± standard error [SE]; $n$ = 4 and 6, respectively), 1% (mean ± SE; $n$ =10 and 16, respectively), and 0.5% (mean ± SE; $n$ = 6 and 10, respectively) CrO on the ears and monitored for ear swelling 3, 6, 12, and 24 hours later. Data are presented as the mean ± SEM (μm) and are a representative of 3 independent experiments. *$P$ < 0.05, between langerin-DTR and corresponding B6 mice.

with our in vitro findings that Zn deficiency augments the release of ATP from irritant-stimulated Pam-212 keratinocytes. In addition, the decreased number of epidermal LCs observed in ZD mice (Figure 4) might also contribute to the increased ATP release from skin organ cultures ex vivo (Figure 2A) as well as the severe and prolonged ICD responses in vivo (Figure 1). Mechanisms include loss of the potent ecto-NTPDase activity of LC-associated CD39, which plays a protective role against ATP-mediated inflammation in ICD responses (28). Taken together, our results suggest that the inflammatory skin manifestations in patients with AE may occur as a result of excessive ICD responses, presumably due to aberrant ATP release upon repeated exposure to various irritants in daily life.

According to our data, Zn deficiency decreases epidermal TGF-β1 expression and its activity in the steady state. While the signaling via TGF-β receptor has been well defined, the homeostatic regulation of TGF-β is largely obscure. So far, the best-characterized regulator (inducer) of TGF-β expression is TGF-β itself (47), and an autocrine production of TGF-β1 is generally required for the homeostasis of various cell types, including LCs (48). Therefore, signaling molecules downstream of TGF-β receptor, such as Smad proteins, are thought to be involved in the regulation of their TGF-β production. Since a number of Zn finger transcription factors (e.g., ZNF580) has been reported to be associated with TGF-β signaling (49), Zn deficiency might decrease the autocrine production of TGF-β1 in LCs and keratinocytes by multiple pathways via those transcription factors.

The present results indicate that Zn deficiency induced the loss of epidermal LCs. Since several lines of evidence have indicated that TGF-β1 governs LC homeostasis (36, 50), the reduced TGF-β1 in epidermis may be, at least in part, responsible for the LC disappearance. The other possible mechanism for LC depletion is apoptosis, because several studies have suggested that Zn is an important physiological regulator of apoptosis (51). Indeed, the incidence of apoptosis in epidermal LCs in ZD mice was increased in the steady state (Supplemental Figure 7A). We also found that murine and human LCs underwent apoptosis when cultured with TPEN at a concentration of 5 μM (Supplemental Figure 7, B and C), while the culture condition did not induce apoptosis in keratinocytes (data not shown), suggesting that LCs are more sensitive to Zn deficiency-induced apoptosis. Taken together with the findings that TGF-β1 has antiapoptosis effects (38, 39), our results suggest that severe Zn deficiency may induce apoptosis in LCs through synergy between its direct effect and the reduced TGF-β1 expression, resulting in the loss of LC networks. Additional studies are needed to determine the impact of TGF-β1 on LC survival in vivo and the paramount mechanism underlying LC disappearance in ZD mice and patients with AE.

A previous study has reported that, in transgenic langerin-DTA mice, depletion of LCs does not affect ICD responses induced by 0.5%–2.5% sodium dodecyl sulfate or 5% BAC (41). In our study using langerin-EGFP-DTR mice, however, the ear swelling response to 1% and 0.5% CrO was significantly increased (Figure 7), consistent with the previous findings that LC-associated CD39 plays a protective role against ATP-mediated inflammation in ICD (28). Nevertheless, both langerin-DTR mice and control mice developed a similar degree of ear swelling after application of 5% CrO (Figure 7), as previously observed in transgenic langerin-DTA mice (41). Since CrO induces ATP release from keratinocytes in a dose-dependent manner (Figure 2), it is possible that an excess ATP release in ICD in response to a high dose of CrO in vivo might be beyond the capacity of NTPDase-dependent hydrolysis by LCs. Alternatively, differences in irritants or depletion timing might explain the phenotypic differences among the LC ablation models (41, 42). Further detailed analysis under different conditions is needed to reveal the functions and significance of LCs in ICD.

## Methods

*Animals and diet.* Five-week-old female BALB/c mice were purchased from Oriental Yeast Co. Ltd. Mice were maintained under specific pathogen-free conditions throughout this study. ZD diet was purchased from CLEA Japan Inc. The mice were fed a powdered ZD diet or control diet from 5 to 11 weeks of age ($n$ = 5–10 per group). Both diets were of almost the same nutritional quality, differing only in terms of Zn content (Zn, 0.11–0.38 mg/100 g in ZD diet, 6.00 mg/100 g in control diet). Langerin-EGFP-DTR mice on a B6 background (provided by Bernard Malissen, Université de la Méditerranée, Aix-en-Provence, Gap and Marseille, France) express a high-affinity human DTR in the langerin locus, as described previously (44). After i.p. injection of 1,000 ng DT in PBS, LCs do not repopulate for at least 4 weeks, while the number of langerin$^+$ dermal DCs in the skin recovers to the basal level about 7 days after depletion by DT (44).

*Patients.* Biopsies were obtained from lesional skin of patients, including those with atopic dermatitis, psoriasis vulgaris, hereditary AE (pretreatment and posttreatment with oral Zn sulfate), and acquired AE. Addition-

ally, control biopsies were obtained from healthy volunteers. The samples were snap frozen in liquid nitrogen and stored at -80°C.

*Reagents and antibodies.* DNFB, CrO, BAC, EPP, TPEN, CBX, and BAPTA-AM were purchased from Sigma-Aldrich. $ZnSO_4$ was purchased from Kanto Chemical Inc. FITC-conjugated anti-human HLA-DR, anti-mouse I-$A^d$, and CD90 (Thy-1) mAbs and PE-conjugated anti-mouse CD11c and I-$A^d$ mAbs were purchased from BD Biosciences. Purified and PE-conjugated anti-human langerin mAbs were purchased from Abcam and R&D Systems, respectively.

*ACD and ICD responses.* For the induction of chemically induced allergic skin inflammation, mice were topically treated with 20 μl 0.5% DNFB dissolved in acetone/olive oil (4:1), which was painted onto the shaved abdomen at days 0 and 1. The ears were then challenged with 10 μl of 0.2% DNFB on the right ear and vehicle alone on the left ear on day 5. For chemically induced irritant skin inflammation, mice received topical application of 1% CrO, 10% BAC, or 30% EPP on the right ear and vehicle alone on the left ear. Swelling responses were quantified (right ear thickness minus left ear thickness) by a third experimenter using a micrometer, as described previously (28). In some experiments, potato apyrase grade VII (0.2 U/ear; Sigma-Aldrich) was injected s.c. into the ear 10 minutes before and 1 hour after CrO painting (28). In experiments with langerin-EGFP-DTR mice, 5%, 1% and 0.5% CrO was painted on the ears.

*Quantification of ATP release from the skin and keratinocytes.* ATP secretion from skin organ culture was quantified, as previously reported (52). Skin samples were taken from both ears immediately. s.c. fat was removed with a scalpel, and the skin explants were prepared by being cut into 8.0-mm circular pieces. The 2 pieces of skin from the 2 ears were floated with the epidermis side upward in 12-well plates containing 4 ml PBS and incubated on ice for 10 minutes. In some experiments, Pam-212 keratinocytes cultured in DMEM medium containing 10% FCS, 10 mM HEPES, 0.25 μg/ml gentamicin, and 2 mM L-glutamine were pretreated with 2 μM TPEN for 6 hours and then cultured with PBS with CrO, BAC, or EPP. ATP concentrations in the supernatants were then quantified using the luciferin-luciferase assay.

*Preparation of epidermal cell suspensions and epidermal sheets.* The ears were removed, mechanically divided into dorsal and ventral cutaneous sheets, and then incubated with a 0.5% solution of trypsin (type XI, Sigma-Aldrich) in PBS for 30 minutes at 37°C to separate the epidermis from the underlying dermis. After removal of the loosened dermis, the epidermal sheets were gently agitated with 0.05% DNase (DN25; Sigma-Aldrich) in PBS for 10 minutes, and the resulting EC suspension was passed through a nylon mesh to remove hair and stratum corneum prior to use. The viability determined by trypan blue exclusion was always more than 90% (53). For immunohistological staining, epidermal sheets were prepared from ear skin by incubation in 0.5 M ammonium thiocyanate (37°C for 20 minutes), fixed in acetone (-20°C for 30 minutes), and rehydrated in PBS (36).

*Preparation of monocyte-derived LCs.* Monocyte-derived LCs were cultured from PBMCs, as described previously (54). Briefly, monocytes were isolated by depletion of magnetically labeled nonmonocytes (Monocyte Isolation Kit II; Miltenyi Biotec) from plastic-adherent PBMCs obtained from healthy blood donors. Monocytes were cultured with 1,000 U/ml recombinant human GM-CSF (R&D Systems), 1,000 U/ml recombinant human IL-4 (R&D Systems), and 10 ng/ml human platelet-derived TGF-β1 (R&D Systems) for 7 days.

*Flow cytometry.* Single-cell suspensions ($5 \times 10^5$) of epidermal sheets, inguinal and axillary lymph nodes, and spleens obtained from ZA and ZD mice (5 mice per group) were stained for LCs with FITC-conjugated anti-I-$A^d$ and PE-conjugated anti-CD11c mAbs or for DETCs with FITC-conjugated anti-Thy-1 mAb for 30 minutes at 4°C. Live/dead discrimination was performed using propidium iodide (Sigma-Aldrich). After washing, samples were analyzed on a FACSCalibur (BD Biosciences). Annexin V-FITC and propidium iodide staining was carried out according to the instructions of BD Pharmingen.

*Histological examination.* Tissue specimens from the ears from ZA or ZD mice were surgically removed immediately after determination of ear swelling, embedded in OCT compound (Tissue-tek), frozen in liquid nitrogen, and stored at -80°C until use. Cryostat sections were fixed in absolute acetone and stained with H&E. For immunohistochemical staining, murine epidermal sheets were stained for LCs and DETCs with PE-conjugated anti-I-$A^d$ mAb or FITC-conjugated anti-Thy-1 mAb, washed, and analyzed by fluorescence microscopy. For human skin samples, cryostat sections were double stained with FITC-conjugated anti-HLA-DR and PE-conjugated anti-langerin mAbs, washed, and analyzed by fluorescence microscopy. For formalin-fixed skin samples, they were stained with anti-HLA-DR and anti-langerin mAbs, incubated with biotinylated goat anti-mouse immunoglobulins, and then incubated with streptavidin-peroxidase. Reactions were developed with aminoethylcarbazole. Sections were incubated with a DAKO LSAB Kit, HRP (DakoCytomation) and then counterstained with Mayer's hematoxylin. Positive (HLA-DR and langerin) cells were counted at high magnification (×400) in 4 different fields, and the average number of positive cells per field was calculated for each sample.

*DNA microarray analysis.* RNA was harvested using TRIzol (Invitrogen) from epidermal sheets obtained from ZA and ZD mice 24 hours after vehicle or CrO exposure. Preparation of cRNA and hybridization of probe arrays (U133.2.plus) was performed according to the manufacturer's instructions (Affymetrix). Data were analyzed according to the MIAME rule. The average μ and SD σ values of ZA and ZD mouse distributions are (-0.049, 1.35) and (-0.041, 1.34), respectively. The accession numbers for each chemokine gene are as follows (GenBank; http://www.ncbi.nlm.nih.gov/genbank): AF065933.1 (*CCL2*), AF128218.1 (*CCL4*), AF128196.1 (*CCL9*), U50712.1 (*CCL12*), NM_011332.1 (*CCL17*), AF099052.1 (*CCL20*), NM_009138.1 (*CCL25*), NM_020279.1 (*CCL28*), NM_008176.1 (*CXCL1*), NM_009140.1 (*CXCL2*), NM_009141.1 (*CXCL5*), NM_008599.1 (*CXCL9*), NM_021274.1 (*CXCL10*), and AF252873.1 (*CXCL14*).

*Quantitative real-time PCR analysis.* Murine epidermal sheets were homogenized in liquid nitrogen using a Mikro-Dismembrator U (Braun Biotech). Total RNA was extracted from Pam-212 keratinocytes or homogenized epidermis using ISOGEN (Nippon Gene), and cDNA was synthesized using the SuperScript system (Invitrogen Life Technologies). Subsequently, relative mRNA expression was determined by real-time PCR using an ABI PRISM 5500 Sequence Detection System (Applied Biosystems) with SYBR Green I Dye (Qiagen). Primers corresponding to mouse chemokines, TGF-β, and G3PDH were designed by TAKARA BIO INC. Ct numbers were derived from the exponential phase of PCR amplification. Fold differences in the expression of gene $x$ in the cell populations $y$ and $z$ were derived by the formula $2^k$, where $k = (Ctx - CtG3PDH)y - (Ctx - CtG3PDH)z$.

*Measurement of TGF-β production and its activity in mucosa and skin.* To measure TGF-β production, skin and mucosa samples were taken from the trunk and the large or small intestine of ZA and ZD mice. The pieces of cutaneous (1.0 × 1.0 $cm^2$) or mucosal (100 mg) tissues were cultured with the epithelial side upward in 24-well plates containing 2 ml RPMI medium (Invitrogen), with 10% FCS, 10 mM HEPES, 0.25 μg/ml gentamicin, and 2 mM L-glutamine for 24 hours. TGF-β production in culture supernatants was measured by ELISA (R&D Systems). In general, TGF-β is secreted in a latent complex in which TGF-β homodimers are noncovalently associated with homodimers of the propeptide called the latency-associated peptide (LAP), and the release of TGF-β from its LAP is required for binding of TGF-β to the cellular receptors (55). To determine TGF-β activity, we used a bioassay using MFB-F11 cells stably transfected with the reporter plasmid containing 12 CAGA boxes (Smad-binding element) fused to a SEAP

reporter gene (56). Briefly, MFB-F11 cells ($4 \times 10^4$ cells/well) in 96-well flat-bottom tissue culture plates were incubated in 50 μl serum-free DMEM for 2 hours, and then skin culture supernatants or TGF-β (10 pg/ml) were added in a 50 μl volume in the presence or absence of 10 μM HTS466284. After 24 hours of incubation, SEAP activity in the culture supernatants was measured using Gene Light 55 (Microtec).

*Statistics.* Significant differences between experimental groups were analyzed by Student's *t* test (1 tailed). *P* values less than 0.05 were considered significant.

*Study approval.* The murine studies were conducted with the approval of and in accordance with the Guidelines for Animal Experiments of the University of Yamanashi. The human study protocol was approved by the institutional review boards of the University Hospital (University of Yamanashi), and informed consent was obtained from all subjects.

## Acknowledgments

We thank Takamitsu Matsuzawa, Rui Aoki, Miyuki Ogino, and Kayoko Ohshimo for technical assistance and Kazutoshi Harada and Naotaka Shibagaki for helpful discussions. We thank Akashi Izumi and Shigeo Ihara for their help with microarray analysis. These studies were supported in part by a grant from the Ministry of Education and Science of the Japanese Government.

Received for publication April 20, 2011, and accepted in revised form November 16, 2011.

Address correspondence to: Tatsuyoshi Kawamura, 1110 Shimokato, Chuo, Yamanashi 409-3898, Japan. Phone: 81.55.273.6766; Fax: 81.55.273.6766; E-mail: tkawa@yamanashi.ac.jp.

1. Prasad AS. Zinc: an overview. *Nutrition.* 1995; 11(1 suppl):93–99.
2. Vallee BL, Auld DS. Cocatalytic zinc motifs in enzyme catalysis. *Proc Natl Acad Sci U S A.* 1993; 90(7):2715–2718.
3. Brown KH, Peerson JM, Rivera J, Allen LH. Effect of supplemental zinc on the growth and serum zinc concentrations of prepubertal children: a meta-analysis of randomized controlled trials. *Am J Clin Nutr.* 2002;75(6):1062–1071.
4. Kitamura H, et al. Toll-like receptor-mediated regulation of zinc homeostasis influences dendritic cell function. *Nat Immunol.* 2006;7(9):971–977.
5. Yamasaki S, et al. Zinc is a novel intracellular second messenger. *J Cell Biol.* 2007;177(4):637–645.
6. Haase H, et al. Zinc signals are essential for lipopolysaccharide-induced signal transduction in monocytes. *J Immunol.* 2008;181(9):6491–6502.
7. Kabu K, et al. Zinc is required for Fc epsilon RI-mediated mast cell activation. *J Immunol.* 2006; 177(2):1296–1305.
8. Maverakis E, et al. Acrodermatitis enteropathica and an overview of zinc metabolism. *J Am Acad Dermatol.* 2007;56(1):116–124.
9. Kury S, et al. Identification of SLC39A4, a gene involved in acrodermatitis enteropathica. *Nat Genet.* 2002;31(3):239–240.
10. Wang K, Zhou B, Kuo YM, Zemansky J, Gitschier J. A novel member of a zinc transporter family is defective in acrodermatitis enteropathica. *Am J Hum Genet.* 2002;71(1):66–73.
11. Kury S, et al. Mutation spectrum of human SLC39A4 in a panel of patients with acrodermatitis enteropathica. *Hum Mutat.* 2003;22(4):337–338.
12. Maggini S, Wenzlaff S, Hornig D. Essential role of vitamin C and zinc in child immunity and health. *J Int Med Res.* 2010;38(2):386–414.
13. Song Y, et al. Dietary zinc restriction and repletion affects DNA integrity in healthy men. *Am J Clin Nutr.* 2009;90(2):321–328.
14. Rink L, Haase H. Zinc homeostasis and immunity. *Trends Immunol.* 2007;28(1):1–4.
15. Murakami M, Hirano T. Intracellular zinc homeostasis and zinc signaling. *Cancer Sci.* 2008; 99(8):1515–1522.
16. Shankar AH, Prasad AS. Zinc and immune function: the biological basis of altered resistance to infection. *Am J Clin Nutr.* 1998;68(2 suppl):447S–463S.
17. Prasad AS. Effects of zinc deficiency on Th1 and Th2 cytokine shifts. *J Infect Dis.* 2000; 182(suppl 1):S62–S68.
18. Prasad AS, et al. Serum thymulin in human zinc deficiency. *J Clin Invest.* 1988;82(4):1202–1210.
19. Richter M, Cantin AM, Beaulieu C, Cloutier A, Larivee P. Zinc chelators inhibit eotaxin, RANTES, and MCP-1 production in stimulated human airway epithelium and fibroblasts. *Am J Physiol Lung Cell Mol Physiol.* 2003;285(3):L719–L729.
20. Zhou Z, Wang L, Song Z, Saari JT, McClain CJ, Kang YJ. Abrogation of nuclear factor-kappaB activation is involved in zinc inhibition of lipopolysaccharide-induced tumor necrosis factor-alpha production and liver injury. *Am J Pathol.* 2004;164(5):1547–1556.
21. von Bulow V, et al. Zinc-dependent suppression of TNF-alpha production is mediated by protein kinase A-induced inhibition of Raf-1, I kappa B kinase beta, and NF-kappa B. *J Immunol.* 2007;179(6):4180–4186.
22. von Bulow V, Rink L, Haase H. Zinc-mediated inhibition of cyclic nucleotide phosphodiesterase activity and expression suppresses TNF-alpha and IL-1 beta production in monocytes by elevation of guanosine 3′,5′-cyclic monophosphate. *J Immunol.* 2005;175(7):4697–4705.
23. King LE, Fraker PJ. Zinc deficiency in mice alters myelopoiesis and hematopoiesis. *J Nutr.* 2002; 132(11):3301–3307.
24. Fraker PJ, King LE, Laakko T, Vollmer TL. The dynamic link between the integrity of the immune system and zinc status. *J Nutr.* 2000;130(5S suppl):1399S–1406S.
25. Lazarowski ER, Boucher RC, Harden TK. Mechanisms of release of nucleotides and integration of their action as P2X- and P2Y-receptor activating molecules. *Mol Pharmacol.* 2003;64(4):785–795.
26. Mizumoto N, Mummert ME, Shalhevet D, Takashima A. Keratinocyte ATP release assay for testing skin-irritating potentials of structurally diverse chemicals. *J Invest Dermatol.* 2003;121(5):1066–1072.
27. Koizumi S, Fujishita K, Inoue K, Shigemoto-Mogami Y, Tsuda M. Ca2+ waves in keratinocytes are transmitted to sensory neurons: the involvement of extracellular ATP and P2Y2 receptor activation. *Biochem J.* 2004;380(pt 2):329–338.
28. Mizumoto N, et al. CD39 is the dominant Langerhans cell-associated ecto-NTPDase: modulatory roles in inflammation and immune responsiveness. *Nat Med.* 2002;8(4):358–365.
29. Koizumi S, Fujishita K, Inoue K. Regulation of cell-to-cell communication mediated by astrocytic ATP in the CNS. *Purinergic Signal.* 2005;1(3):211–217.
30. Grabbe S, Schwarz T. Immunoregulatory mechanisms involved in elicitation of allergic contact hypersensitivity. *Immunol Today.* 1998;19(1):37–44.
31. Zhang L, Tinkle SS. Chemical activation of innate and specific immunity in contact dermatitis. *J Invest Dermatol.* 2000;115(2):168–176.
32. Meller S, et al. Chemokine responses distinguish chemical-induced allergic from irritant skin inflammation: memory T cells make the difference. *J Allergy Clin Immunol.* 2007;119(6):1470–1480.
33. Olson TS, Ley K. Chemokines and chemokine receptors in leukocyte trafficking. *Am J Physiol Regul Integr Comp Physiol.* 2002;283(1):R7–R28.
34. Ohara H, et al. Gene expression profiling defines the role of ATP-exposed keratinocytes in skin inflammation. *J Dermatol Sci.* 2010;58(2):143–151.
35. Merad M, Ginhoux F, Collin M. Origin, homeostasis and function of Langerhans cells and other langerin-expressing dendritic cells. *Nat Rev Immunol.* 2008;8(12):935–947.
36. Borkowski TA, Letterio JJ, Farr AG, Udey MC. A role for endogenous transforming growth factor beta 1 in Langerhans cell biology: the skin of transforming growth factor beta 1 null mice is devoid of epidermal Langerhans cells. *J Exp Med.* 1996;184(6):2417–2422.
37. Tesseur I, Zou K, Berber E, Zhang H, Wyss-Coray T. Highly sensitive and specific bioassay for measuring bioactive TGF-beta. *BMC Cell Biol.* 2006;7:15.
38. Riedl E, Strobl H, Majdic O, Knapp W. TGF-beta 1 promotes in vitro generation of dendritic cells by protecting progenitor cells from apoptosis. *J Immunol.* 1997;158(4):1591–1597.
39. Ohtani T, et al. TGF-beta1 dampens the susceptibility of dendritic cells to environmental stimulation, leading to the requirement for danger signals for activation. *Immunology.* 2009;126(4):485–499.
40. Wilson D, Varigos G, Ackland ML. Apoptosis may underlie the pathology of zinc-deficient skin. *Immunol Cell Biol.* 2006;84(1):28–37.
41. Kaplan DH, Jenison MC, Saeland S, Shlomchik WD, Shlomchik MJ. Epidermal langerhans cell-deficient mice develop enhanced contact hypersensitivity. *Immunity.* 2005;23(6):611–620.
42. Kissenpfennig A, et al. Dynamics and function of Langerhans cells in vivo: dermal dendritic cells colonize lymph node areas distinct from slower migrating Langerhans cells. *Immunity.* 2005;22(5):643–654.
43. Bennett CL, et al. Inducible ablation of mouse Langerhans cells diminishes but fails to abrogate contact hypersensitivity. *J Cell Biol.* 2005;169(4):569–576.
44. Honda T, et al. Compensatory role of Langerhans cells and langerin-positive dermal dendritic cells in the sensitization phase of murine contact hypersensitivity. *J Allergy Clin Immunol.* 2010;125(5):1154–1156.
45. Chai F, Truong-Tran AQ, Evdokiou A, Young GP, Zalewski PD. Intracellular zinc depletion induces caspase activation and p21 Waf1/Cip1 cleavage in human epithelial cell lines. *J Infect Dis.* 2000; 182(suppl 1):S85–S92.
46. Kolenko V, et al. Dead or dying: necrosis versus apoptosis in caspase-deficient human renal cell carcinoma. *Cancer Res.* 1999;59(12):2838–2842.
47. Kim SJ, Jeang KT, Glick AB, Sporn MB, Roberts AB. Promoter sequences of the human transforming growth factor-beta 1 gene responsive to transforming growth factor-beta 1 autoinduction. *J Biol Chem.* 1989;264(12):7041–7045.
48. Kaplan DH, Li MO, Jenison MC, Shlomchik WD, Flavell RA, Shlomchik MJ. Autocrine/paracrine TGF-beta1 is required for the development of epidermal Langerhans cells. *J Exp Med.* 2007;204(11):2545–2552.
49. Luo Y, Hu W, Xu R, Hou B, Zhang L, Zhang W. ZNF580, a novel C2H2 zinc finger transcription factor, interacts with TGF-beta signal molecule SMAD2. *Cell Biol Int.* 2011;35(11):1153–1157.
50. Hacker C, et al. Transcriptional profiling identifies Id2 function in dendritic cell development. *Nat Immunol.* 2003;4(4):380–386.

51. Chai F, Truong-Tran AQ, Ho LH, Zalewski PD. Regulation of caspase activation and apoptosis by cellular zinc fluxes and zinc deprivation: A review. *Immunol Cell Biol.* 1999;77(3):272–278.
52. Denda M, Inoue K, Fuziwara S, Denda S. P2X purinergic receptor antagonist accelerates skin barrier repair and prevents epidermal hyperplasia induced by skin barrier disruption. *J Invest Dermatol.* 2002;119(5):1034–1040.
53. Kawamura T, Azuma M, Kayagaki N, Shimada S, Yagita H, Okumura K. Fas/Fas ligand-mediated apoptosis of murine Langerhans cells. *J Dermatol Sci.* 2000;22(2):96–101.
54. Ogawa Y, Kawamura T, Kimura T, Ito M, Blauvelt A, Shimada S. Gram-positive bacteria enhance HIV-1 susceptibility in Langerhans cells, but not in dendritic cells, via Toll-like receptor activation. *Blood.* 2009;113(21):5157–5166.
55. Schmierer B, Hill CS. TGFbeta-SMAD signal transduction: molecular specificity and functional flexibility. *Nat Rev Mol Cell Biol.* 2007;8(12):970–982.
56. Nakamura Y, et al. House dust mite allergen Der f 1 can induce the activation of latent TGF-beta via its protease activity. *FEBS Lett.* 2009;583(12):2088–2092.

# Artemin causes hypersensitivity to warm sensation, mimicking warmth-provoked pruritus in atopic dermatitis

**Hiroyuki Murota, MD, PhD,[a] Mayuko Izumi, MSc,[a] Mostafa I. A. Abd El-Latif, MD, PhD,[a,b] Megumi Nishioka, MD,[a] Mika Terao, MD, PhD,[a] Mamori Tani, MD,[a] Saki Matsui, MD,[a] Shigetoshi Sano, MD, PhD,[c] and Ichiro Katayama, MD, PhD[a]** *Osaka and Kochi, Japan, and Cairo, Egypt*

**Background: Itch impairs the quality of life for many patients with dermatoses, especially atopic dermatitis (AD), and is frequently induced by a warm environment.**
**Objective: To determine the mechanism underlying itch induction by warmth, we focused on artemin, a member of glial cell line–derived neurotrophic factors (GDNFs).**
**Methods: A gene array assay revealed that artemin was expressed in substance P–treated dermal fibroblasts. The expression of artemin in healthy and AD-lesional skin was evaluated with immunohistochemistry and *in situ* hybridization. The impact of fibroblast-derived artemin on the proliferation and morphology of neural cell was investigated *in vitro*. To confirm the involvement of artemin in skin sensibility, wild-type and GDNF family receptor α3 knockout mice were employed for sensory examination.**
**Results: Artemin-expressing fibroblasts accumulated in skin lesions of patients with AD. Artemin induced cell proliferation of a neuroblastoma cell line *in vitro*, and intradermal injection of artemin in mice resulted in peripheral nerve sprouting and thermal hyperalgesia. Artemin-treated mice demonstrated scratching behavior in a warm environment, but mice deficient for GDNF family receptor α3, a potent artemin receptor, did not show this behavior. Furthermore, the escaping response to heat stimulus was attenuated in GDNF family receptor α3 knockout mice, suggesting that artemin may contribute to sensitivity to heat.**
**Conclusion: These data suggest that dermal fibroblasts secrete artemin in response to substance P, leading to abnormal peripheral innervation and thermal hyperalgesia. We hypothesize that artemin lowers the threshold of temperature-dependent itch sensation and might therefore be a novel therapeutic target for treating pruritic skin disorders, including AD. (J Allergy Clin Immunol 2012;130:671-82.)**

*Key words:* *Artemin, fibroblast, substance P, atopic dermatitis, itch, nerve fiber, warmth*

Itch is the major symptom of inflammatory skin diseases and impairs the quality of life of patients.[1-3] Because itch-induced scratching behavior worsens skin conditions and leads to a vicious itch-scratching cycle,[2,4,5] antipruritic treatment plays a central role in these diseases.[6] An accurate understanding of the mechanisms that cause itch in various skin disorders will contribute to formulate therapies. Several factors are reported to exacerbate itch clinically, and heat-/warmth-provoked itching, in particular, occurs with high frequency.[4,7] Although excessive response to warmth or light mechanical stimuli has been thought of as alloknesis caused by central/peripheral processing sensitization,[4,7] the relationship between heat sensation and itch is less well understood. In previous reports, pruritogens such as histamine and substance P (SP) are described as mediators of alloknesis.[8-10] These factors will contribute to cause alloknesis via affecting various types of cells.[11] However, specific factors that induce warmth-evoked itch remain obscure. In the face of this concern, we focused on the fact that cutaneous nerve fibers are ordinarily localized in dermis and made a hypothesis that dermal fibroblast-derived factors might affect cutaneous nerve fibers and cause alloknesis to warm sensation. To investigate this hypothesis, expression profiling was performed to identify genes induced by histamine or SP treatment in fibroblasts. The results led us to focus on *de novo* artemin gene transcription in fibroblasts after SP stimulation.

Artemin is a member of the glial cell line–derived neurotrophic factor (GDNF)-related family, which includes GDNF, neurturin, and persephin.[12-15] Members of this family are thought to act through a multireceptor complex composed of GDNF family receptor α (GFRα) and the receptor tyrosine kinase product of the c-ret proto-oncogene.[16,17] Four distinct GFRαs (GFRα1-4) have been described in the literature as preferentially binding to GDNF family proteins.[18] Artemin appears to be the only member of the GDNF family that binds to and activates the GFRα3-receptor tyrosine kinase product of the c-ret proto-oncogene receptor complex[18] and is expressed in smooth muscle cells of the vessels during embryogenesis and has been considered to be a guidance factor encouraging sympathetic axonal projections.[19] Although the expression of artemin was found in a number of adult tissues, its function remains obscure, especially in skin.[18]

Here, we examine the involvement of endogenously expressed artemin from dermal fibroblasts in skin innervation and skin sensibility.

From [a]the Department of Dermatology, Course of Integrated Medicine, Graduate School of Medicine, Osaka University; [b]the Department of Dermatology, Cairo University; and [c]the Department of Dermatology, Kochi University.

This study was supported by the Ministry of Education, Culture, Sports, Science and Technology, Japan.

Disclosure of potential conflict of interest: The authors declare that they have no relevant conflicts of interest.

Received for publication February 18, 2012; revised April 20, 2012; accepted for publication May 23, 2012.

Available online July 4, 2012.

Corresponding author: Hiroyuki Murota, MD, PhD, Department of Dermatology, Course of Integrated Medicine, Graduate School of Medicine, Osaka University, 2-2, Yamadaoka, Suita-Shi, Osaka, Japan 565-0871. E-mail: h-murota@derma.med.osaka-u.ac.jp.

0091-6749/$36.00



http://dx.doi.org/10.1016/j.jaci.2012.05.027

*Abbreviations used*
AD: Atopic dermatitis
CM/SP: Conditioned medium derived from SP-treated NHDF
GDNF: Glial cell line–derived neurotrophic factor
GFRα: GDNF family receptor α
GFRα3 KO: GFRα3 knockout
NGF: Nerve growth factor
NHDF: Normal human dermal fibroblast
PDF: Primary dermal fibroblast
rARTN: Recombinant artemin
SP: Substance P
TRPV1: Transient receptor potential vanilloid 1

## METHODS

### Cell culture

A cultured normal human dermal fibroblast (NHDF) and SH-SY5Y, a neuroblastoma cell line, were purchased from Health Science Research Resources Bank (Osaka, Japan). Primary dermal fibroblasts (PDFs) were isolated from human adult skin samples. NHDF, PDFs, and HaCaT cells were cultured in Dulbecco modified Eagle medium (Gibco-BRL, Gaithersburg, Md) containing 10% fetal bovine serum (BioWhittaker, Inc, Walkersville, Md) and streptomycin at 37°C in a 5% $CO_2$ atmosphere. Murine embryonic fibroblastswere isolated and cultured as previously described.[20] SH-SY5Y was cultured in a 1:1 mixture of Essential Eagle's medium and Ham's F12 medium (both from Gibco-BRL) containing 10% fetal bovine serum. Normal human epidermal keratinocytes purchased from DS Pharma Biomedical (Osaka, Japan) were cultured in human keratinocyte serum-free medium (DS Pharma Biomedical).

### Mice

Ten-week-old female mice were used in all experiments. C57BL/6 mice were purchased from Japan Clea (Osaka, Japan). GFRα3 knockout (GFRα3 KO) mice were described previously[21] and were a kind gift from Developmental Genetics Group, Graduate School of Frontier Biosciences, Osaka University. Mice were maintained in our pathogen-free animal facility. All animal care was in accordance with the institutional guidelines of Osaka University.

### Slide culture of neuroblastoma cell line

SH-SY5Y cells were seeded in Lab-Tek chamber slides (NALGENE Labware, Rochester, NY). After 1 day in culture, cells were cultured with 50 ng/mL recombinant artemin (rARTN; R&D Systems, Minneapolis, Minn) or conditioned medium derived from $1 \times 10^{-6}$ or $1 \times 10^{-12}$ mol/L SP-treated NHDF after 12 hours of incubation. Three days after the addition of these factors, cells were photographed with a BZ-8000 microscope (Keyence, Osaka, Japan).

### Cell proliferation assay

The proliferation rate was determined by using the cell proliferation ELISA BrdU assay kit (Cell Proliferation ELISA, BrdU, Roche, Mannheim, Germany). SH-SY5Ycells were cultured in the rARTN and SP-treated NHDF-derived conditioned medium with or without antiartemin antibody (R&D Systems), anti-GDNF antibody (Abcam, Cambridge, United Kingdom; ab10835), and anti–nerve growth factor (NGF)-β antibody (Chemicon, Temecula, Calif; AB1528) in a 96-well microplate at 37°C for 24 hours. Subsequently, BrdU incorporation was measured according to the manufacturer's instruction.

### Histologic analysis

Samples of human and murine skin were cut on a cryostat to 20-μm thick sections.

For human healthy control skin and atopic dermatitis (AD), nummular eczema, prurigo nodularis, and psoriasis skin lesion biopsies, the antibodies used were goat antiartemin (sc-9331, Santa Cruz Biotechnology, Santa Cruz, Calif), rabbit antiartemin, goat anti-GFRα3 (both from R&D Systems), PGP-9.5 (Chemicon; AB1761), and vimentin (Dako, Carpentaria, Calif). Secondary antibodies were conjugated to Alexa Fluor 488 or 594 (Invitrogen, Carlsbad, Calif). For SP staining, 4-μm paraffin sections were incubated with primary antibodies (Abcam) and stained with the streptavidin-biotin amplification EnVision system (Dako).

For murine samples, the hindpaws of C57BL6 mice or GFRα3KO mice were intradermally injected once with 20 μL of $1 \times 10^{-4}$ mol/L SP and 0.2 μg/20 μL recombinant mouse artemin (1085-AR/CF, R&D Systems). The dose setting of artemin injection was based on a previous report.[22] One day after administration, skin biopsy was performed at the injection site. The sections were incubated with primary antibody for SP (Abcam) and PGP9.5 (Chemicon) and visualized with fluorescein isothiocyanate or Alexa Fluor 594. Images were captured with a BZ-8000 microscope (Keyence).

### Behavioral analysis

Response to infrared heat stimulus was measured with the tail flick test (Tail-flick unit; Ugo Basile, Comerio VA, Italy) and Hargreaves test (37370-Planter Test instrument, Ugo Basile). Mechanosensation was evaluated by Planter Test instrument (Ugo Basile). The effect of artemin and SP on thermal hyperalgesia was evaluated by using the Hargreaves test.[23] Animals were acclimated to the apparatus for 30 minutes before testing. The apparatus was set at a laser intensity of 60 (temperature after 10, 20, and 30 seconds was 42.0°C, 47.5°C, and 51.0°C, respectively), and testing was performed by using repeated measures (3-5 measures per foot) of the glabrous hindpaw skin. Three response times were averaged for each animal.

In experiments examining mouse behavior at warm temperatures, 0.2 μg/20 μL artemin or vehicle was given intradermally in interscapular on a Monday through Thursday schedule for a total of 4 injections over 2 weeks. One day after the final administration, mice were placed in constant warm temperature and a humid place (38°C and 60%, respectively). Mice were videotaped for 15 minutes following installation, and the time spent scratching or wiping was measured as described previously.[24] The transient receptor potential vanilloid 1 (TRPV1) antagonist, capsazepine (10 mg/kg), was administered intraperitoneally with a volume of 1 mL/kg before 5 minutes of investigation as described previously.[25]

### RT-PCR

Total RNA was extracted with an RNeasy Mini kit (QIAGEN Gmbh, Hilden, Germany), according to the protocol provided by the manufacturer. First-strand cDNA was synthesized with an RT-PCR kit (Stratagene, La Jolla, Calif) by using oligo dT primers. The primers used for RT-PCR are presented in Table I. The ARTN primer set used for RT-PCR was purchased from SuperArray (Frederick, Md).

### Real-time PCR

The levels of artemin, GDNF, and NGF mRNAs were analyzed by using Power SYBR Green PCR Master Mix (Applied Biosystems, Foster City, Calif) according to the manufacturer's protocols. Glyceraldehyde-3-phosphate was used to normalize mRNA levels. Sequence-specific primers are shown in Table I. The artemin primer set was purchased from SuperArray (Frederick, Md). Real-time PCR was performed on an ABI Prism 7000 sequence detector (Applied Biosystems).

### Western blot analysis

NHDFs were washed with PBS twice, and approximately $5 \times 10^5$ cells were solubilized at 4°C in a lysis buffer. The protein extracts were analyzed with an antiartemin antibody (Santa Cruz). An antiactin antibody (Chemicon) was used as a control. For detection of Ser696-phosphorylated c-Ret,

**TABLE I.** Primer sequences for PCR

| Gene | Accession no. | Sequences | |
|---|---|---|---|
| For RT-PCR | | | |
| *NGF* | NM_002506.2 | Sense | 5′-GAC AGT GTC AGC GTG TGG GTT-3′ |
| | | Antisense | 5′-CCC AAC ACC ATC ACC TCC TT-3′ |
| *GDNF* | NM_000514.3 | Sense | 5′-TTC GCG CTG AGC AGT GAC-3′ |
| | | Antisense | 5′-TAC ATC CAC ACC TTT TAG CGG-3′ |
| *Neurturin* | NM_004558.3 | Sense | 5′-CCT CAG TGC TCT GCA GCT C-3′ |
| | | Antisense | 5′-TCG TGC ACC GTG TGG TAG-3′ |
| *GFRα1* | NM_005264.4 | Sense | 5′-ACC AGC GTG TCC AAT GAT GT-3′ |
| | | Antisense | 5′-AGG CAG TCA GCG TAG TTT TC-3′ |
| *GFRα2* | NM_001495.4 | Sense | 5′-GCT GGC ATG ATT GGG TTT GA-3′ |
| | | Antisense | 5′-TTG GAG TTG TTG GCC TTC AG-3′ |
| *GFRα3* | NM_001496.3 | Sense | 5′-GTG TGA AAT GCT GGA AGG GT-3′ |
| | | Antisense | 5′-TCA GGA GCA GAA TCA AGG GA-3′ |
| *GFRα4* | NM_022139.3 | Sense | 5′-CTC TCC ATA CTT CCT GTC CT-3′ |
| | | Antisense | 5′-CTA CAA AAG TGA CCC TCT CC-3′ |
| *GAPDH* | NM_002046.3 | Sense | 5′-ACC ACA GTC CAT GCC ATC AC-3′ |
| | | Antisense | 5′-TCC ACC ACC CTG TTG CTG TA-3′ |
| For real-time PCR | | | |
| *NGF* | NM_002506.2 | Sense | 5′-CAG TTT TAC CAA GGG AGC AGC TT-3′ |
| | | Antisense | 5′-CAA CAT GGA CAT TAC GCT ATG CA-3′ |
| *GDNF* | NM_000514.3 | Sense | 5′-TTC GCG CTG AGC AGT GAC T-3′ |
| | | Antisense | 5′-GCC ATT TGT TTA TCT GGT GAC CTT-3′ |

*GAPDH*, Glyceraldehyde-3-phosphate.

anti-phospho(Ser696) c-Ret antibody (Upstate, Charlottesville, Va) and anti-Ret antibody (Abcam) were used as primary antibodies.

## Macroarray gene assay

Murine embryonic fibroblasts were prepared and cultured by using a previously described method.[21] At the subconfluent stage, cells were incubated with or without $1 \times 10^{-6}$ mol/L SP or histamine (Sigma, St Louis, Mo) for 6 hours and total RNAs were isolated with an RNeasy kit (QIAGEN GmbH). The Panorama Mouse Cytokine Gene Array (Sigma) assay was performed according to the manufacturer's instructions. Gene expression signals were quantitated with a BAS5000 (Fujifilm, Tokyo, Japan).

## *In situ* hybridization

Tissue sections were prepared and hybridized as described previously.[26] DIG-labeled riboprobes for artemin (human artemin transcript variant 2, accession: NM_057091, sequence position: 1452-1873) were prepared by using DIG RNA Labeling Mix (Roche, Indianapolis, Ind). A negative control riboprobe was purchased from Genostaff Co, Ltd (Tokyo, Japan). The sections were counterstained with Kernechtrot stain solution (Mutoh, Tokyo, Japan), dehydrated, and then mounted with Malinol (Mutoh).

## Statistic analysis

Statistical significance was examined by unpaired *t* test or Bonferroni's multiple comparison test. Graph bars in the figures present mean ± SD.

## Study approval

Human tissue samples were obtained with written informed consent, and the studies were approved by the institutional review board of Osaka University Hospital.

# RESULTS

## Artemin is induced in SP-treated dermal fibroblasts

The results in macroarray gene assays prompted us to focus on artemin, which is expressed in SP-treated fibroblasts, but not in mock- or histamine-treated murine embryonic fibroblasts (Fig 1, *A*). We then examined the expression of histamine and other members of the GDNF family in human dermal fibroblasts and keratinocytes by RT-PCR (Fig 1, *B*). Artemin expression was detected in normal human epidermal keratinocytes and spontaneously immortalized keratinocyte, HaCaT cells, but not in untreated PDFs or commercially available NHDF. GDNF expression was relatively high in NHDF and lower in PDFs and normal human epidermal keratinocytes. Neurturin mRNA was not detected in these cell types. To verify whether SP treatment influences the expression of artemin, GDNF, and NGF in NHDFs, mRNAs were examined by quantitative real-time PCR after treatment with various concentrations of SP (Fig 1, *C*). We found that the expression of artemin mRNA increased in an SP dose-dependent fashion. In contrast, the expression level of GDNF was not affected by SP treatment. The expression of NGF mRNA was upregulated, with peak expression at $1 \times 10^{-12}$ mol/L SP (Fig 1, *C*). Western blotting analysis revealed that artemin protein could be detected 12 hours after SP treatment and became undetectable again after 24 hours (Fig 1, *D*).

## Artemin accumulates in the dermis of AD skin lesions

To assess artemin expression levels in itchy skin diseases, skin sections derived from healthy controls and patients with AD were immunohistochemically stained to detect artemin (Fig 2, *A*). The epidermis and the dermis of AD skin lesions showed an intense staining pattern for artemin, whereas the pattern was weak in healthy control skin. Accumulation of artemin was also observed in nummular eczema lesional skin, and in prurigo nodularis and psoriasis, but with less intense staining (see Fig E1 in this article's Online Repository at www.jacionline.org). To determine the source of artemin, costaining with vimentin (Fig 2, *B*) and CD34 (Fig 2, *C*) was performed. Dermal fibroblasts (vimentin$^+$),

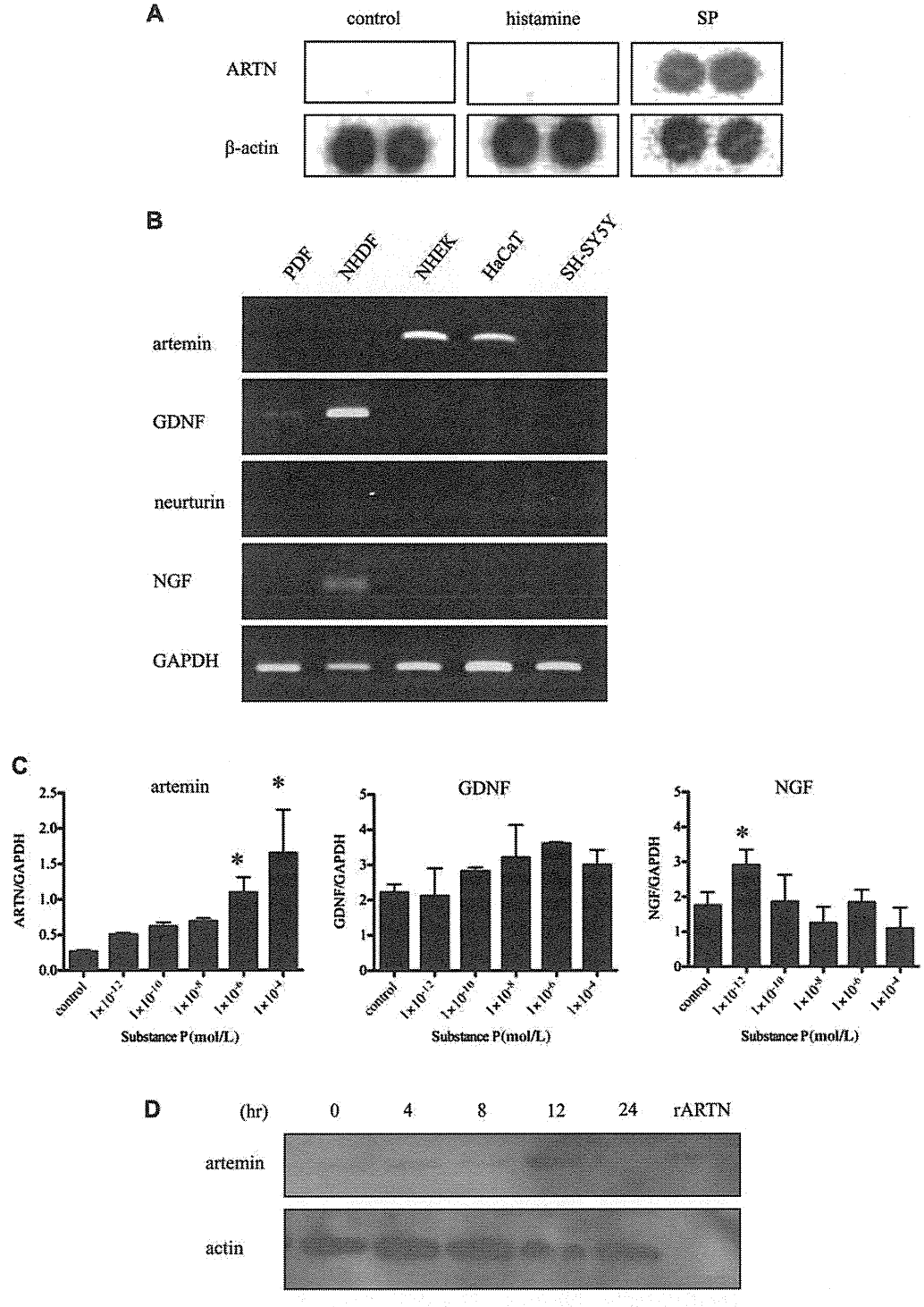


**FIG 1.** SP-treated fibroblasts express artemin. **A,** Result of macrogene array. Control: vehicle-treated. **B,** RT-PCR analysis of GDNF family, and NGF expression PDFs, NHDFs, and NHEKs. The data shown are representative of 2 independent experiments. **C,** Real-time PCR results in NHDF treated with various concentrations of SP for 6 hours. $*P < .05$. **D,** Sequential expression levels of artemin were examined by Western blot after treatment with $1 \times 10^{-6}$ mol/L SP. *ARTN*, Artemin; *GAPDH*, glyceraldehyde-3-phosphate; *NHEKs*, normal human epidermal keratinocytes.

but not endothelial cells ($CD34^+$), in AD skin lesions costained for artemin. Although the number of dermal fibroblasts differed between healthy and diseased skin, the weak staining intensity of artemin in prurigo nodularis (also known as dermatitis with increased number of fibroblast[27]) indicates that the accumulation of artemin in the dermis of lesional skin is not simply a consequence of the altered number of dermal fibroblasts (see Figs E1 and E2 in this article's Online Repository at www.jacionline.org). *In situ*

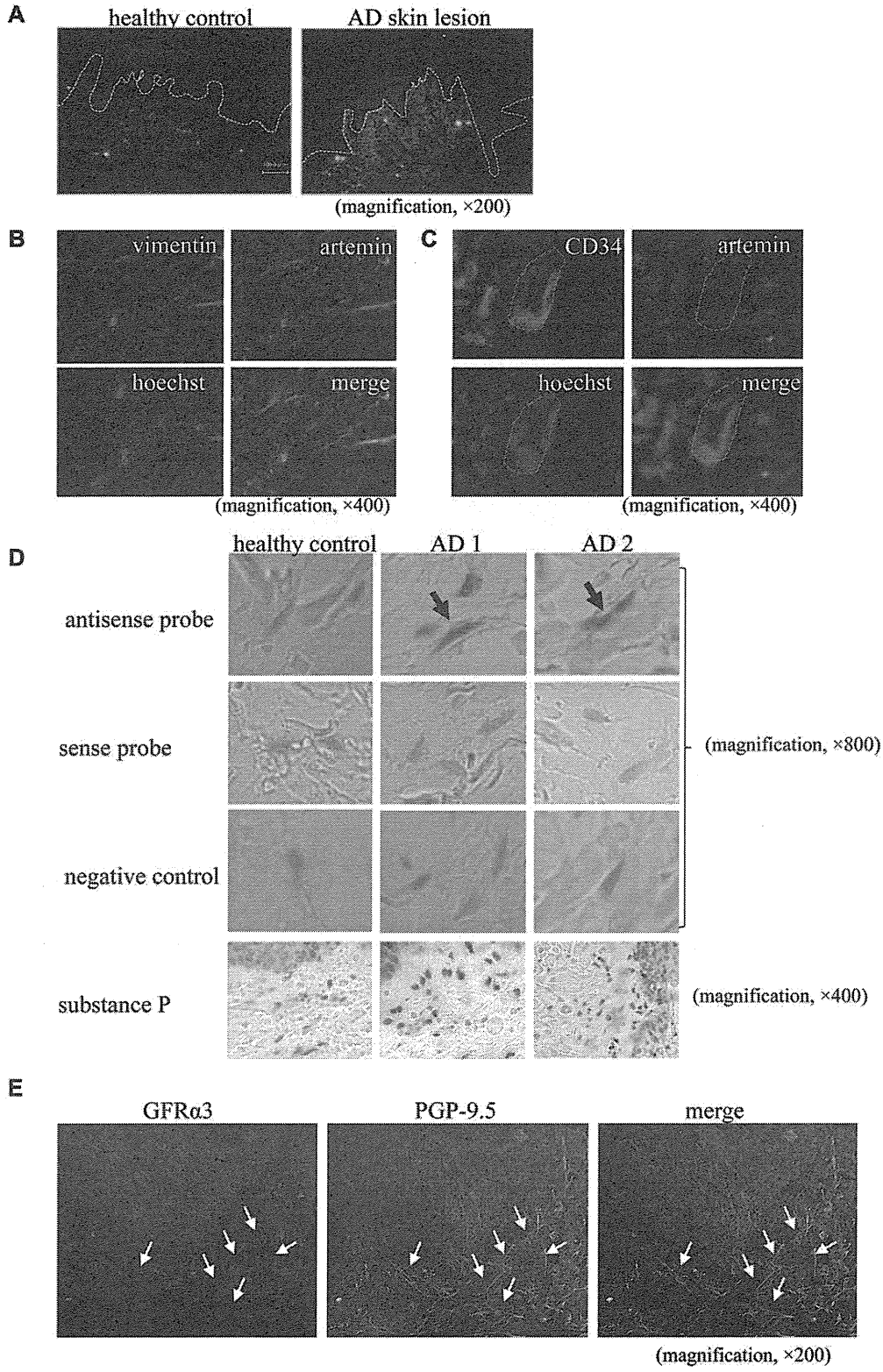


**FIG 2.** Accumulation of artemin in dermal fibroblasts from AD skin lesions. **A,** Healthy skin and an AD skin lesion (with disease duration of about 1 month) were stained for artemin. *Dashed white lines* represent the epidermal-dermal junction. AD skin lesion was costained for vimentin and artemin **(B)** or CD34 and artemin **(C)**. Hoechst: Hoechst 33342. *Dashed lines* represent the vascular wall (Fig 2, *C*). **D,** *In situ* hybridization for artemin. Positive signal appeared with blue (indicated by *arrows*). The disease duration was 4 days for AD1 and about 1 month for AD2. The same skin sections were immunostained for SP. **E,** Lesional skin with disease duration of about 1 month was immunolabeled with PGP-9.5 and GFRα3. *Arrows* indicate costained nerve fibers.

hybridization also revealed reproducible expression of artemin mRNA expression in the dermal fibroblasts of AD skin lesions but not in healthy skin (Fig 2, *D*). Increased numbers of SP-positive peripheral nerve fibers were also observed in the AD skin lesions (Fig 2, *D,* bottom).

Next, we were interested in determining whether artemin modulates the peripheral projection patterns of neurons. As expected, artemin-labeled, highly fluorescent dermal areas in AD skin lesions showed massive sprouting of PGP-9.5–positive peripheral neurons (see Fig E3 in this article's Online Repository at www.jacionline.org). Colabeling with anti-GFRα3 antibody proved that the sprouting nerve fibers in AD skin lesions were GFRα3-positive (Fig 2, *E*).

## Artemin derived from SP-treated NHDFs induces strong differentiation and proliferation response in neuroblastoma cells

To compare the ability of the fibroblast-derived neurotrophic factors to influence a differentiation response in peripheral neurons, SH-SY5Y was cultured in conditioned medium derived from NHDF cultured with or without SP (Fig 3). The expression levels of GFRα1, GFRα2, and GFRα3 in SH-SY5Y cells suggest that this cell line responds to both GDNF and artemin (Fig 3, *A*). There was no significant difference in the morphology or proliferation of cells cultured with conditioned medium derived from mock-treated NHDF compared with those derived from fresh medium culture (Fig 3, *B* and *C*). An increase in the size of SH-SY5Y was observed with the conditioned medium derived from SP-treated NHDF (CM/SP) as well as rARTN treatment, but not in SH-SY5Y alone treated with SP (Fig 3, *B*). A BrdU incorporation assay revealed that CM/SP augmented the proliferation of SH-SY5Y (Fig 3, *C*). The role of artemin in CM/SP-induced SH-SY5Y proliferation was verified in experiments with an artemin neutralization antibody. Artemin neutralization inhibited the rARTN-induced proliferation of SH-SY5Y cells, whereas an isotype matched control antibody did not (see Fig E4 in this article's Online Repository at www.jacionline.org). As expected, artemin neutralization attenuated the CM/SP-induced proliferation of SH-SY5Y, whereas GDNF and NGF neutralization did not (Fig 3, *C*). Artemin neutralization also inhibited the phosphorylation of the receptor tyrosine kinase product of the c-ret proto-oncogene in SH-SY5Y cells cultured with rARTN or CM/SP (Fig 3, *D*).

## Intradermal administration of artemin promotes peripheral nerve fiber sprouting and intraepidermal neurite outgrowth

The finding of high GFRα3 expression on sprouted peripheral nerve fibers led us to examine the possibility that artemin contributes to the peripheral nerve fiber sprouting. Wild-type mice were intradermally injected with artemin or SP 2 times per week for 2 weeks, and SP- or artemin-injected sites showed an increased number of peripheral nerve fibers, whereas nontreated (control) or vehicle-injected sites did not (Fig 4, *A*). Interestingly, artemin injection sites also displayed intraepidermal neurite outgrowth. As expected, the SP- or artemin-mediated nerve sprouting response was decreased in GFRα3KO mice (Fig 4, *B*), as was intraepidermal neurite outgrowth in artemin-injected sites (Fig 4, *B*).

## Artemin is involved in thermal hyperalgesia

To explore whether artemin affects the cutaneous sensitivity to environmental stimuli, the intensity of perception was evaluated in GFRα3KO mice. The intensity of mechanosensation in GFRα3KO mice was comparable to that in wild-type mice (Fig 5, *A*). Next, thermal hyperalgesia was assessed by using Hargreaves test and a tail-flick test (Fig 5, *B* and *C*). In both experiments, the withdrawal latency time was prolonged at temperatures greater than 40°C, indicating that GFRα3KO mice have thermal hypoalgesia. To investigate the effect of artemin on thermal hyperalgesia, artemin-treated wild-type mice were examined for heat susceptibility by using Hargreaves test. As expected, a single administration of artemin induced thermal hyperalgesia (Fig 5, *D*).

SP has long been thought to elicit thermal hyperalgesia.[28] We also found that SP treatment shortened hindpaw withdrawal latency time after 12 hours (Fig 5, *E*). To confirm the involvement of artemin in SP-induced thermal hyperalgesia, artemin-neutralizing antibody was administered (Fig 5, *F*). Further prolongation of withdrawal latency time in artemin-neutralized, SP-treated mice was comparable to that in mice treated with SP alone, demonstrating a key role for artemin in SP-induced thermal hyperalgesia.

## Administration of artemin to mice induced abnormal behavior in a warm environment

If artemin regulates thermal susceptibility, artemin-injected mice might display altered behavior when exposed to a warm environment. To verify this, mice received subcutaneous injection of artemin or vehicle into the interscapular region and were placed at an environmental temperature of 38°C, and their behavior was recorded with video imaging for 15 minutes. Surprisingly, artemin-injected mice showed wiping of the cheek (not the injection site) with forefoot starting about 3 minutes after being placed in a warm environment (see Video E1 in this article's Online Repository at www.jacionline.org). This abnormal behavior with stops at short intervals persisted to the end of the video recording and was confirmed by 2 repeated experiments (n = 3 for each experiment) (Fig 6, *A*). Vehicle-injected mice did not show any abnormal behavior in the 38°C environment. Both vehicle- or artemin-injected mice did not show behavioral differences at room temperature (data not shown). To confirm the involvement of GFRα3-mediated signaling in artemin-induced abnormal behavior, artemin-injected GFRα3KO mice were examined in the same behavioral assay. We found that artemin-injected GFRα3KO mice behaved like the vehicle-injected GFRα3KO mice and vehicle-injected wild-type mice (Fig 6, *B*) and did not display abnormal behavior. Capsazepine, a selective TRPV1-inhibitor, did not affect the artemin-induced abnormal behavior (Fig 6, *C*).

## DISCUSSION

Artemin derived from SP-treated dermal fibroblasts was accumulated in AD-lesional skin and found to induce cutaneous nerve sprouting and cause rubbing behavior mimicking scratching warmth-evoked itch in mice.

In our study, artemin was strongly expressed on the dermis of skin biopsy slices from patients with AD. The homogenous staining pattern of artemin in the dermis is assumed to reflect the